

7-13-2022

# Modeling Postfire Effects on Snow Albedo and Forest Recovery Over a Chronosequence of Burned Forests in the Triple Divide Region of the Rocky Mountains

Anton J. Surunis  
*Portland State University*

Follow this and additional works at: [https://pdxscholar.library.pdx.edu/open\\_access\\_etds](https://pdxscholar.library.pdx.edu/open_access_etds)



Part of the [Environmental Sciences Commons](#)

**Let us know how access to this document benefits you.**

---

## Recommended Citation

Surunis, Anton J., "Modeling Postfire Effects on Snow Albedo and Forest Recovery Over a Chronosequence of Burned Forests in the Triple Divide Region of the Rocky Mountains" (2022). *Dissertations and Theses*. Paper 6193.  
<https://doi.org/10.15760/etd.8046>

This Thesis is brought to you for free and open access. It has been accepted for inclusion in Dissertations and Theses by an authorized administrator of PDXScholar. Please contact us if we can make this document more accessible: [pdxscholar@pdx.edu](mailto:pdxscholar@pdx.edu).

Modeling Postfire Effects on Snow Albedo and Forest Recovery over a Chronosequence  
of Burned Forests in the Triple Divide Region of the Rocky Mountains

by  
Anton J. Surunis

A thesis submitted in fulfillment of the  
requirements for the degree of

Master of Science  
in  
Environmental Science and Management

Thesis Committee:  
Kelly E. Gleason, Chair  
Paul Loikith  
Yangdong Pan

Portland State University  
2022

© 2022 Anton J. Surunis

## ABSTRACT

Wildfires impact snow albedo, forest cover, and forest structure and thus snow melt rate and snowpack supply for as long as 15 years following burn. These effects have not been quantified at fine spatial resolutions and long time periods at a watershed scale. I modeled the effects of postfire effects on snow albedo, snow-mass energy balance, and resulting snow-water equivalent (SWE) depth over a long-time scale and at a fine spatial resolution. Using a spatially and temporally distributed snow evolution model called SnowModel, I modeled postfire effects on snow albedo and forest structure over postfire recovery within 8 forest fires between 2000 and 2020 in a region in Northwestern Wyoming. SnowModel does not currently incorporate the effects of postfire effects on snow albedo, forest structure nor the recovery of the postfire effects, so I developed and incorporated postfire snow albedo decay functions from Gleason and Nolin (2016) into SnowModel and developed a 15-year postfire recovery of postfire effects on snow albedo and forest structure parameterization informed by remotely-sensed measurements of surface snow albedo from the MODIS-MOD10A1 dataset. I then compared the parameterized model (postfire albedo) with a base model to quantify changes in peak SWE, snow volume, and snow disappearance date (SDD) due to postfire effects on snow and recovery within the burn regions and at the watershed scale for up to 20 years following fire. To partition the postfire impacts on snow due to forest structure from the albedo impacts, I also parameterized a third model with only forest structure impacts (postfire forest) and compared the results with the postfire albedo model and the base

model. My hypothesis was that modeled results would show significant and lasting alterations in peak SWE, total snow volume, and SDD for up to 15 years following fire. Postfire parameterizations caused peak SWE losses of between 2.81% and 31.91% (474K m<sup>3</sup> to 12.7M m<sup>3</sup>) and an average 9.93 to 87.97% reduction in ablation season SWE in the year immediately following fire. Immediately following fire, snow disappearance occurred 33 (SD: 3 days) to 58 days (SD: 9 days) earlier than in the base model. Over recovery, losses in total SWE and peak SWE, and shifts in disappearance date tended to shrink relative to the losses observed immediately following fire, but remained negative throughout. In two fires modeled for the entire 15 year postfire recovery period, the greatest losses in peak SWE did not occur immediately following fire, but instead 4-9 years following fire. Postfire effects on snow summed over the entire 15-year recovery period caused total reductions in peak SWE of between 0.76% and 12.45% (5.5M m<sup>3</sup> and -20.5M m<sup>3</sup>) over 1 to 15 years following fire - losses between 2 and 18 times greater than the losses incurred in the first year immediately following ignition. Postfire impacts were most severe in burns occurring at lower elevation. Beyond 15 years following fire, postfire effects on snow persisted due to the shift from forest to open meadow over the course of the 15-year recovery period. The Boulder fire (ignition date:2000) showed significant increases in snow volume (+2.32%; +196K m<sup>3</sup>) 16 years following fire while the Green Knoll fire (ignition date: 2001) showed peak SWE losses (-2.20%; -241K m<sup>3</sup>) 16 years following fire. Postfire impacts in the Lower Granite Creek subbasin, a heavily burned watershed (Ryan et al., 2011) within the study region (43% burned over 20 years), caused average annual reductions in ablation season (May 1<sup>st</sup>) SWE of  $-6.30 \pm 6.95\%$  ( $5.9M m^3 \pm 6.5M m^3$ ). Postfire effects in the Lower Granite Creek subbasin caused

earlier melting of 5.85% of snowpack over 20 years in total, an amount equal to 94M m<sup>3</sup> of additional runoff added to the watershed over 20 years. Overall, parameterizations of postfire impacts and recovery showed significant changes in snow volume and spring snowmelt following fire that lasted 16+ years beyond the initial ignition date.

Quantifying the changes in snow accumulation and snowmelt due to severe wildfire using postfire recovery parameterizations will provide critical understanding needed for anticipating wildfire effects on water supply under a changing climate and increasingly severe fire regime.

## ACKNOWLEDGEMENTS

I would like to thank my committee, Dr. Kelly Gleason, Dr. Yangdong Pan, and Dr. Paul Loikith, all of whom have provided valuable support, helpful feedback, and excellent tutelage throughout my time at Portland State University. They have all helped me to become a better scientist over the last two years and have enabled my success in more ways than I can discuss here.

I would like to thank the National Aeronautics and Space Administration's Terrestrial Hydrology Program for funding my research under Award #80NSSC19K0002.

I am also grateful for the support of my lab mates, Megan Guinn, Nani Ciafone, and Max Gersh who have all given me unending support and insightful advice in my work and, most importantly, close friendship.

I would like to thank Dr. Glen Liston and Dr. Ryan Crumley who took time out of their busy schedules many times to help me run and troubleshoot SnowModel.

I would like to thank my parents, Christ Surunis, Andrea Anton, and my grandfather, Ronald Bretall, who all instilled the value and importance of pursuing a career in science from a very young age.

Finally, I am eternally grateful for the support of my fiancé, Allison Jones Kruse, who upended her life in San Francisco to come to Portland, OR with me so that I could pursue my dreams of becoming an environmental scientist. This work would not have been possible without her love and support, her patience with my late nights at work, and a steady supply of coffee to help me get over those late nights.

Table of Contents	
<b>ABSTRACT</b> .....	<b>i</b>
<b>ACKNOWLEDGEMENTS</b> .....	<b>iv</b>
<b>LIST OF TABLES</b> .....	<b>vii</b>
<b>LIST OF FIGURES</b> .....	<b>viii</b>
<b>LIST OF ACRONYMS</b> .....	<b>ix</b>
<b>INTRODUCTION</b> .....	<b>1</b>
<i>Study Design</i> .....	6
<i>Study Region</i> .....	6
<i>Parameterization Background</i> .....	7
<i>Model Descriptions</i> .....	9
<i>Research Goals</i> .....	10
<b>METHODOLOGY</b> .....	<b>13</b>
<i>Study Region</i> .....	13
<i>MODIS Albedo Decay Modeling</i> .....	14
<i>SnowModel Input Data Retrieval</i> .....	14
<i>Snow-Water Equivalent Assimilation</i> .....	17
<i>SnowModel Calibration</i> .....	18
<i>Parameterizations of postfire albedo decay, land cover change, and recovery</i> .....	21
<i>SnowModel Batch Runs</i> .....	25
<i>Analysis of Model Results: Snow Volume and Disappearance Date Calculations</i> .....	26
<i>Analysis of Model Results: Spatial and Daily Variability of SWE over Season and Recovery</i> .....	28
<i>Quantification of Watershed Scale Impacts</i> .....	29
<i>Statistical Analysis</i> .....	30
<i>Model Validation</i> .....	31
<b>RESULTS</b> .....	<b>33</b>
<i>Immediate Postfire Effects on Snow Volume and Snow Disappearance Date</i> .....	33
<i>Immediate Postfire Effects on Seasonal Snow-Water Equivalent</i> .....	34
<i>Postfire Effects on Snow Volume and Snow Disappearance Date over Recovery</i> .....	37
<i>Recovery of Postfire Effects on Seasonal Snow-Water Equivalent</i> .....	39

<i>Effects of Postfire Impacts and Recovery on Total Snow Volume .....</i>	<i>41</i>
<i>Effects of Postfire Impacts and Recovery at the Watershed Scale .....</i>	<i>42</i>
<i>Model Validation.....</i>	<i>43</i>
<b>DISCUSSION .....</b>	<b>45</b>
<i>Postfire Forest Structure Impacts on Snow Hydrology .....</i>	<i>46</i>
<i>Postfire Snow Albedo Impacts on Snow Hydrology.....</i>	<i>46</i>
<i>Variability in Postfire Effects on Snow Volume over Season and Recovery.....</i>	<i>49</i>
<i>Total Effects of Postfire Impacts on Snow .....</i>	<i>51</i>
<i>Model Validation.....</i>	<i>52</i>
<i>Limitations and Future Work .....</i>	<i>54</i>
<b>CONCLUSION .....</b>	<b>58</b>
<b>FIGURES AND TABLES .....</b>	<b>60</b>
<b>REFERENCES.....</b>	<b>74</b>
<b>APPENDIX A: LONG-TERM POSTFIRE RECOVERY TREND METHODS .....</b>	<b>80</b>
<b>APPENDIX B: TUKEY ANALYSIS OF LONG TERM POSTFIRE RECOVERY TRENDS .....</b>	<b>82</b>
<b>APPENDIX C: FIGURES AND TABLES .....</b>	<b>85</b>

## LIST OF TABLES

<b>Table 1.</b> List of meteorological stations used as the meteorological forcing data input or as validation data in SnowModel.....	63
<b>Table 2.</b> Table showing the final performance statistics of SnowModel following pre-parameterization calibrations.....	63
<b>Table 3.</b> Calculations of the differences in volumetric SWE (<1 year postfire, total, and per period) and differences in snow disappearance date (SDD) between the base model and burn-recovery parameterized model.....	64
<b>Table 4.</b> Average annual proportional peak SWE loss between the postfire effect and recovery model and the baseline model.....	72
<b>Table 5.</b> Results of the model validation using field measurements of SWE collected from six of the burns between February and March of 2019.....	73

## LIST OF FIGURES

<b>Figure 1.</b> Map and table of study region, meteorological stations, and burns modeled....	60
<b>Figure 2.</b> Conceptual model of the postfire effects parameterized in SnowModel and simplified methodology.....	61
<b>Figure 3.</b> Subset of plots used in the calibration of SnowModel.....	62
<b>Figure 4.</b> Matrix of rasters of the Green Knoll fire (Ignition Year: 2001) showing the change in snow-water equivalent depth (SWED) between the base model and parameterized model.....	65
<b>Figure 5.</b> A combined raster/nivea matrix similar to Figure 7 for the Roosevelt fire (Ignition Year: 2018).....	66
<b>Figure 6.</b> A combined raster/nivea matrix similar to Figure 7 for the Boulder fire (Ignition Year: 2000).....	67
<b>Figure 7.</b> A combined raster/nivea matrix similar to Figure 7 for the Bull fire (Ignition Year: 2010).....	68
<b>Figure 8.</b> A combined raster/nivea matrix similar to Figure 7 for the Cliff Creek fire (Ignition Year: 2016).....	69
<b>Figure 9.</b> A combined raster/nivea matrix similar to Figure 7 for the Horsethief Canyon fire (Ignition Year: 2012).....	70
<b>Figure 10.</b> A combined raster/nivea matrix similar to Figure 7 for the Horsethief Canyon fire (Ignition Year: 2012).....	71
<b>Figure 11.</b> A combined raster/nivea matrix similar to Figure 7 for the Purdy fire (Ignition Year: 2006).....	72
<b>Figure 12:</b> Spatial analysis of watershed scale impacts of postfire effects and recovery in the Lower Granite Creek subbasin (HUC12) during the ablation period (May 1 <sup>st</sup> ) for every modeled year.....	73

## LIST OF ACRONYMS

### *Statistical Metrics:*

NSE = Nash-Sutcliffe Efficiency

PBIAS = Percent Bias

$R^2$  = Coefficient of Determination

RMSE = Root Mean Square Error

RSR = Root Square Error

### *Data Sources:*

CDO = Climate Data Online

CFSv2 = Climate Forecast System version 2

GMTED = Global Multi-resolution Terrain Elevation Data

MODIS = Moderate Resolution Imaging Spectroradiometer

MTBS = Monitoring Trends in Burn Severity

NASA = National Aeronautics and Space Administration

NCEP = National Centers for Environmental Prediction

NOAA = National Oceanic and Atmospheric Administration

NRCS = National Resources Conservation Service

NWCC = National Weather and Climate Center

RAWS = Remote Automatic Weather Stations

SNOTEL = Automated Snow Telemetry sites

SRTM = Shuttle Radar Topography Mission

USDA = United States Department of Agriculture

WRCC = Western Regional Climate Center

### *General Terms:*

LGC = Lower Granite Creek HUC12 subbasin

SDD = Snow Disappearance Date

SHD = Snow-holding Depth

SWE = Snow-Water Equivalent

SWED = Snow-Water Equivalent Depth

YPF = Years Post Fire

## INTRODUCTION

The American West stores much of its water in snowpack. Warming due to climate change and subsequent changes to snowpack energy balance have impacted zones of snow accumulation and the supply of water to areas downstream (Barnett et al, 2005; Mote et al, 2018; Luce et al., 2009; Luce et al., 2013). Approximately 50-70% of water in the Intermountain West falls as snow, with the flora, fauna, and human populations relying on the slow and steady melting of this snow as a source of water in the dry periods of spring and summer (Serreze et al., 1999). Due to global warming, it is predicted that the spring streamflow maximum in the western US will occur about one-month earlier than it does today by the year 2050 (Barnett et al., 2005; Barnett et al., 2008). Current water storage infrastructure cannot accommodate such a shift in streamflow regime. Excess water would be released into oceans, resulting in a 10-20% reduction in hydropower and significant impacts to important aquatic populations such as salmon (Payne et al., 2004; Barnett et al., 2005).

Western forest fires occur predominately in the heavily-forested seasonal snow zone where as much as 50% of western snow falls (Gleason and Nolin, 2013). The frequency, severity, and extent of forest fire in the American West has been increasing due to rising air temperatures and subsequent effects on seasonal snowpack and summertime soil moisture (Westerling, 2016). Watersheds burned for as little as 19% of their watershed area have significant reductions in river flow in the following melt season resulting in greater soil moisture deficits and drier summer conditions in forests, making these watersheds more prone to future wildfire (Helema et al., 2018).

Wildfire in the seasonal snow zone modifies forest structure and increases black carbon inputs to snow, altering the snowpack energy balance and snow ablation (Gleason et al., 2019). Canopy removal by wildfire reduces shading, subjecting greater surface areas of snow to increased solar shortwave radiative inputs and increasing wind-driven sublimation losses (Ueyama et al., 2014). Canopy removal also reduces longwave radiative inputs from vegetation, but in continental snowpack these reductions can often be counteracted by the additional inputs of solar radiative forcing due to reduced shading and increased wind ablative losses (Musselman et al., 2008; Varhola et al., 2010; Lundquist et al., 2013). In continental regions, where temperatures are colder and longwave radiative inputs from vegetation are reduced, additional solar radiative inputs from reductions in shading tend to outweigh the losses in longwave radiative inputs from canopy removal and result in a net increase in shortwave radiative forcing on snowpack (Musselman et al., 2008; Varhola et al., 2010; Lundquist et al., 2013).

Forest fires in the seasonal snow zone introduce black carbon and burned woody debris into snowpack, reducing snow albedo and increasing shortwave radiative forcing on snowpack (Gleason et al., 2019). Following wildfire, surface snow albedo is reduced directly through the deposition of light absorbing impurities on the surface of snowpack, resulting in increased shortwave radiative forcing on snow (Gleason et al., 2019). Snow albedo is also reduced indirectly by enhancing the rate of snow metamorphosis and subsequent albedo decay. Following snowfall, fine snow grains metamorphose into coarser grains over time, exhibiting reduced surface area and fewer snow-air interfaces, decreased capacity to reflect or refract incoming photons, and overall lower surface snow albedo (Wiscombe and Warren, 1980). The addition of black carbon on snow from

charred forests enhances the rate at which snow metamorphosis occurs following fresh snowfall and the corresponding rate of snow albedo decay over time (Gleason and Nolin, 2016). Together, forest fires impact snow hydrology through direct and indirect reductions in snow albedo and canopy removal, resulting in increased solar forcing on snow, altered snowpack energy balance, decreased peak snow-water equivalent (SWE), and earlier snow disappearance dates (SDD) (Gleason et al., 2013; Gleason et al., 2019; Gleason and Smoot, 2021).

Reductions in snow albedo from wildfire last up to 15 years following burn and have collectively resulted in a four-fold increase in solar forcing on snow in burned forests in the western US since 1999 (Gleason et al., 2019). Postfire effects on snow result in losses in mid-winter snowpack volume, accelerated snowmelt during ablation, and significantly earlier SDD (Gleason et al., 2013; Gleason et al., 2019; Smoot & Gleason, 2021). A comparison of SNOTEL sites within burn regions to reference sites located outside fire showed significant reductions in peak SWE and significantly earlier SDD in seasonal snow zones for up to 10 years following fire (Smoot & Gleason, 2021). However, efforts to assess the impacts of wildfire on snow at the watershed scale using SNOTEL data alone are limited as SNOTEL stations are situated in specific sites chosen primarily for ease of access and to limit public disturbance (Meromy et al., 2012); thus, these data do not necessarily represent the variability in snowpack conditions across a basin (Meromy et al., 2012; Molotch and Bales, 2005). Further, many western forest fires occur in remote, high-elevation regions, making direct measurements of postfire effects the snowpack across the watershed scale and over many years following fire difficult, dangerous, and costly.

The difficulty in quantifying postfire impacts on snow over large temporal and spatial scales using in-situ measurements make remotely sensed measurements a valuable tool in monitoring snow properties in remote regions over broad spatial scales. Recent research by Gersh et al. (2022) utilized remotely sensed measurements of snow albedo from the National Aeronautics and Space Administration's (NASA) Moderate Resolution Imaging Spectroradiometer (MODIS) instrument's snow albedo product (MOD10A1) to analyze trends in the long-term recovery of snow albedo following wildfire in the Triple Divide Region of Wyoming (Gersh et al., 2022). The results of this research showed that snow albedo and landcover steadily recovered back to an unburned open meadow state over the course of 15 years, with much of the recovery occurring in the first 10 years following the initial burn (Gersh et al., 2022). The rapid return time and long mission lengths of satellite observations make remotely sensed observations an important data source in assessing long-term postfire recovery trends over large spatial scales. However, assessment of fine-scale snow albedo trends using these data are limited by coarse resolutions and the presence of obstructions such as clouds or canopy. MODIS-MOD10A1 data are provided at a low spatial resolution of 500m and are not able to measure snow albedo values through clouds or other obstructions such as canopy cover (Hall and Riggs, 2007; Armitage et al., 2013; Riggs et al. 2017). Measurements of snow albedo can be influenced by fine scale landcover variability resulting in mixed pixels that do not accurately represent the albedo in a given grid cell (e.g., patchy snow cover can artificially reduce albedo measurements) (Cescatti et al., 2012; Campagnolo et al., 2016) and variability in cloud cover can result in long periods where little to no data can be retrieved from a particular study region (Hall and Riggs, 2007; Armitage et al., 2013;

Riggs et al. 2017). The limited spatial extent of in-situ measurements and coarse resolution of remotely sensed measurements make physically-based snow evolution models that incorporate such data an important tool in quantifying the long-term effects of wildfire on snow at a watershed scale.

This study modeled the postfire effects on snow using a spatially distributed snow-evolution model called SnowModel. SnowModel is a process-based model that uses first-order physics to simulate snow accumulation; blowing-snow redistribution and sublimation; snow-density evolution; and snowpack melt over spatially varying elevation and landcover grids driven by temporally varying meteorological forcing fields (Liston and Elder, 2006a; Liston and Elder, 2006b; Liston et al., 2007). SnowModel was used in this study because of its basis in first-order physics, ready customizability, and extensive validation in forested, montane seasonal snowpack similar to my study region (Hiemstra et al., 2006; Liston and Elder, 2006a; Liston and Elder, 2006b; Liston et al., 2007; Liston et al., 2008; Sextone et al., 2018). SnowModel utilizes four sub-models in a hierarchal modeling structure: *MicroMet*, *EnBal*, *SnowPack-ML*, and *SnowTran-3D*. *MicroMet* spatially interpolates meteorological forcing data from met stations observations and/or modeled reanalysis met outputs of air temperature, precipitation, wind speed, wind direction, air pressure, and relative humidity (Liston and Elder, 2006b). Using a spatially-weighted Barne's interpolation method, *MicroMet* produces a meteorological forcing field for every cell in the simulation for every time step (Liston and Elder, 2006b). *MicroMet* also estimates incoming shortwave and longwave radiation inputs in each cell using solar calculations based on the latitude of the study region and parametrizations of cloudiness (Liston and Elder, 2006b). *EnBal* utilizes the outputs of *MicroMet* and

physics-based mass energy balance equations to calculate the snow mass-energy balance of the snowpack within every cell at every time step of the simulation (Liston and Hall, 1995). *SnowTran-3D* is a three-dimensional model that incorporates the wind-flowing forcing field from *MicroMet* and topographical and vegetation inputs to compute redistribution of snow due to wind and loss of snow by saltation and wind-induced sublimation (Liston et al., 2007). *SnowPack-ML* computes snow-density through temperature- and compaction-based snow-density evolution (Liston and Elder, 2006a). *SnowPack-ML* can be run using a single layer or up to 12 distinct layers and simulates cold content, permeability, and liquid water release from the snowpack within each cell for every time step (Liston and Elder, 2006a). The mechanistic nature of SnowModel's calculations and its high customizability make SnowModel a powerful tool in quantifying modified snow-mass energy balance regimes such as those outlined above.

#### *Study Design*

#### *Study Region*

To date, research has shown that postfire effects of wildfires occurring in the seasonal snow zone affect snow hydrology for many years following the initial burn (Gleason et al., 2013; Gleason et al., 2019; Smoot & Gleason, 2021). However, no studies have quantified postfire effects on snow hydrology at a fine spatial resolution and over the decades-long postfire recovery period using a physically based snow evolution model. This study modeled and quantified postfire impacts on peak SWE, total snow volume, and SDD in a heavily-burned area within the Triple Divide region of northwestern Wyoming. The Triple Divide region of Wyoming has experienced a significant increase in drought and corresponding wildfire occurrence over the last

decade. Wyoming, like much of the western United States, faces the growing threat of dramatic declines in snowpack, more rapid snow melt, drier forests, and resulting increased wildfire risk (Westerling, 2016; Kulakowski & Jarvis, 2011; West et al., 2015). According to NOAA's state climate summary for Wyoming, severe state-wide drought in recent years has resulted in a significant increase in wildfire occurrence (Frankson et al., 2017). In 2012 alone, Wyoming experienced over half a million acres of burned area, a 7-fold increase in the typical historical average. While often suffering from severe droughts in the Great Plains region of the state, the mountainous regions receive more the 200 inches of snowfall per year making Wyoming a major source of water for states and river basins that extend beyond the state borders. Rainfall in Wyoming helps to feed four major river basins including the Green-Colorado river basin, Missouri-Mississippi river basin, Great Salt Lake river basin, and Columbia river basin, broadening the implications of impacts to Wyoming's water supply to regions outside the state boundaries (Frankson et al., 2017). The study region investigated in this study (Figure 1) resides within the Triple Divide region of Wyoming. Although only 8 burns within my study region are modeled here, 26 burns in total occurred in my study region between 2000 and 2020. Many of these burns overlap with the seasonal snow zone, making it a prime location for modeling the postfire effects of wildfire on the snow-mass energy balance.

### *Parameterization Background*

This research quantified postfire effects on snow hydrology over the postfire recovery period within a region of the Triple Divide (see *Methodology: Study Region*) by incorporating a postfire effect on snow albedo and forest structure and recovery parameterization into SnowModel. A simplified conceptual model of the postfire effects

on snow, forest structure, and recovery parameterization as well as the general modeling process can be found in Figure 2. The postfire effect on snow albedo decay and forest structure and recovery model utilized a parameterization of postfire effects on snow albedo and snow albedo decay from Gleason and Nolin (2016) and a postfire forest structure degradation and snow albedo recovery model informed by long-term trends in MODIS-derived landscape snow albedo (LSA) from Gersh et al. (2022). The parameterization of postfire effects on snow albedo and snow albedo decay was drawn from a study by Gleason and Nolin (2016) which derived empirical snow albedo decay functions from broadband snow albedo measurements taken in adjacent burned and unburned forested sites in the Shadow Lake burn region (ignition date: 2011) in the Oregon Cascades up to 3 years following fire. The parameterizations from this study characterized snow albedo decay as an exponential function of days since snowfall for both burned and unburned forested sites and for both positive net energy balance periods (accumulation) and negative net energy balance periods (ablation) respectively for a total of four snow albedo decay functions (Gleason & Nolin, 2016). The long-term (1-15 years postfire) snow albedo recovery trends were informed from a study by Gersh et al. (2022) which characterized postfire snow albedo recovery over many years following fire in a chronosequence of eight burns occurring in the Triple Divide region of Wyoming between 2000 and 2018, the same burns modeled in my study. The study by Gersh et al. (2022) utilized MODIS-MOD10A1 measurements of landscape snow albedo (LSA) values taken from within the eight burn regions for up to 15 years following fire and determined, through Tukey analysis, that LSA values within the burn regions shifted to LSA values similar to that of unburned open regions over the course of 15 years

following fire. The findings of these two studies provided the basis for postfire and unburned snow albedo ranges and snow albedo decay (Gleason & Nolin, 2016) and informed the long-term postfire recovery of snow albedo towards an unburned forested state over the course of 15 years following fire (Gersh et al., 2022).

### *Model Descriptions*

Using the above parameterization, I developed three models to quantify how postfire effects on snow albedo, snow albedo decay, and forest structure degradations alter snow volume and snowmelt timing over the decades-long postfire recovery period. The three models included a base model, a postfire forest model, and a postfire albedo model. A summary of each of the three models and their purpose follows, but more detailed descriptions of each model can be found in the Methodology section.

The base model consisted of a default SnowModel run from which to compare and contrast the results of the postfire forest and postfire albedo models. The default version of SnowModel does not include snow albedo decay functionality, so the base model was supplemented with a modified time-decay of albedo parameterization from Gleason & Nolin (2016) which applied different time-decay of snow albedo to grid cells depending on their landcover type (forested or unforested) and the season of the current time step (accumulation or melting season). All equations relating to burned grid-cells were removed from the base model. In short, the base model represented a simulation of the study region for 20 years with no postfire effects incorporated.

The postfire forest model consisted of the base model with the addition of time-varying postfire forest degradation parameterizations that simulated the degradation of forest structure over 15 years following fire towards that of an open meadow, but with no

postfire effects on snow albedo or snow albedo decay included. The postfire forest model allowed for compartmentalization of postfire effects on snow hydrology due to forest structure changes and postfire effects on snow hydrology due to postfire effects on snow albedo and snow albedo decay. In short, the postfire forest model simulated only the postfire effects of forest structure degradation over 15 years without postfire effects on snow albedo.

The postfire albedo model consisted of both the time-decay of albedo parameterizations from Gleason & Nolin (2016) as well as the forest structure degradation parameterizations from the postfire forest model. In short, this model simulated the postfire effects on snow albedo, snow albedo decay, and forest structure and recovered these parameters to the snow albedo ranges, snow albedo decay trends, and forest structure of that of an open meadow over the course of 15 years following fire.

### *Research Goals*

Following calibration of the base model, parameterizations for the postfire forest and postfire albedo models were applied and each of these models was run for 20 years (from 2000 to 2020). The results of the postfire albedo model and postfire forest model were then compared with the results of the base model to quantify postfire effects on snow hydrology (peak SWE, total snow volume, and SDD) over decades following fire in critical headwaters. By incorporating postfire effects on snow albedo and forest structure and the associated recovery into a mechanistic model, I was able to quantify the impacts that wildfire has on snow hydrology across a chronosequence of eight burns within the study region over the 20-year modeling period. Specifically, I addressed the following research questions:

1. What are the immediate (1-year postfire) volumetric and proportional differences in peak SWE and SDD caused by postfire snow albedo and forest structure modifications?
2. How do postfire effects on snow albedo and forest structure impact snow volume throughout the snow season (accumulation, start of ablation, and ablation) and how do impacts on peak SWE, seasonal snow volume, and SDD change over the course of the postfire recovery many years following fire?
3. What are the total volumetric and proportional impacts of postfire effects on snow albedo and forest structure degradation on peak SWE summed over 15 years following fire and are there any lasting impacts on peak SWE and SDD beyond 15 years following fire?
4. How do postfire effects on snow albedo and forest structure impact total ablation season snow volume at a watershed scale over the entire 20-year modeling period?

Regarding these research questions, I hypothesized that:

1. Parameterizations of postfire effects on snow albedo and forest structure will cause reductions in peak SWE and shift SDD earlier with the greatest reductions in peak SWE and earliest shifts in SDD occurring immediately following fire.
2. Parameterizations of postfire effects on snow albedo and forest structure will cause increases in snow volume in burn regions during the accumulation season, decreases in snow volume at the start of ablation and during ablation, and reductions in seasonal snow volume, peak SWE and shifts in SDD will all lessen over years since fire.

3. Parameterizations of postfire effects on snow albedo and forest structure will cause net reductions in peak SWE and total snow volume when summed over 15 years of postfire recovery and changes in peak SWE and SDD will still be observed beyond 15 years following fire due to changes in landcover.
4. Parameterizations of postfire effects on snow albedo and forest structure will cause annual reductions in ablation season snow volume at the watershed scale.

Understanding and quantifying how postfire effects on snow albedo and forest structure impact snow hydrology over many years following fire is vital as the Intermountain West continues to warm and wildfires increase in occurrence, extent, duration, and severity. The modeling approach and findings discussed here will help to improve understanding of the broad scale and lasting implications of forest fire on snow in headwaters critical for spring and summertime water supply.

## METHODOLOGY

### *Study Region*

To model and quantify the impacts of postfire effects on snow albedo and forest structure on snow hydrology, I investigated an area within the Triple Divide region of Wyoming. SnowModel requires the user to first define a rectangular study region in which to perform grid-based calculations. To define this region, I first selected eight burns which occurred in the Triple Divide region of Wyoming. The eight fires were chosen due to their progressive ignition dates providing a chronosequence of burns occurring in the region over 20 years and due to the availability of ground validation data available for several of these fires. The modeling region was then defined by calculating a minimum bounding rectangle within ArcGIS containing the eight fires plus a 2km buffer using burn perimeters from MTBS (MTBS, 2017). The final modeling region contained an area of 7677 square kilometers with the eight selected burns resulting in a total of 564 square kilometers of burned area (Figure 1).

Based on a preliminary analysis of meteorological and landcover data collected within the study region between 2000 and 2020 (more information on this data is provided in the *SnowModel Input Data Retrieval* subsection) the study domain had an average daily air temperature of  $1.57 \pm 19.24$  degrees Celsius over the 20-year modeling period and received an average of  $2.00 \pm 7.96$  mm daily precipitation. The modeling region is largely forested, consisting of 60% forested land and 40% unforested land (35% shrub, grassland, and agricultural, 0.006% urban, and 4% bare rock). The forested land is pine-dominated, of which the most common species are Lodgepole Pine (*Pinus contorta*) and Whitebark Pine (*Pinus albicaulis*). The average elevation of the modeling area was

2503 ± 680m with a minimum and maximum elevation of 1727m and 3596m respectively.

### *MODIS Albedo Decay Modeling*

Prior to running SnowModel and applying the postfire recovery parameterization, long-term recovery trends in snow albedo and landcover recovery were determined using MODIS-MOD10A1 snow albedo data from the study region from Gersh et al. (2022). Using these data, I performed a Tukey analysis comparing landscape snow albedo (LSA) values from within the burn regions to LSA values in 5 km unburned buffer regions around the fires over many years following fire. Following this analysis, it was found that LSA values within the burn regions shifted away from the LSA values of unburned forest and approached LSA values closer to those of unburned open regions over the course of 15 years following fire. In short, by investigating trends in postfire LSA for up to 15 years following fire, I found that, following fire, snow albedo values within burn regions trended to those of open meadows rather than those of pre-burn forests. This finding informed the postfire recovery parameterization in such a way that forest structure within burned forests would recover to open meadows over 15 years rather than back to forest. Further information on MODIS-measured albedo analysis can be found in Appendices A and B.

### *SnowModel Input Data Retrieval*

SnowModel requires three major inputs: meteorological forcing data, a topographic elevation raster, and a landcover classification raster. Meteorological forcing data was retrieved from both automated weather stations and modeled reanalysis data. In-

situ meteorological forcing data from automated weather stations were retrieved from the United States Department of Agriculture (USDA) National Resources Conservation Service's (NRCS) automated Snow Telemetry (SNOTEL) network (USDA-NRCS, 2020) via the National Weather and Climate Center (NWCC) data retrieval tool. SNOTEL data were supplemented with additional in-situ weather data from the Western Regional Climate Center's (WRCS) Remote Automated Weather Station (RAWS) network (WRCS, 2021), and the National Oceanic and Atmospheric Administration's (NOAA) Climate Data Online (CDO) network (NOAA-CDO, 2022) to capture a wider range of weather variability over elevation. Information on the specific stations used and relevant metadata can be found on Table 1. In-situ meteorological data was further supplemented with modeled re-analysis meteorological data from NOAA's Climate Forecast System version 2 (CFSv2) data sourced through Google Earth Engine.

SNOTEL data from the USDA-NRCS (USDA-NRCS, 2020) were retrieved from the nine SNOTEL stations within the study region using the USDA-NRCS data retrieval tool. Daily values of air temperature, precipitation, wind speed, wind direction, and relative humidity were used as well as station metadata required for input into SnowModel (elevation and geographic coordinates). In addition to these input data, SNOTEL-measured values of SWE were also retrieved for later calibration of the modeled results.

RAWS weather data were retrieved from the two stations within the study region using the *RAWSmet* package in *R*. RAWS stations are automated weather stations established throughout the US to monitor air quality, fire risk, and assist in land management practices (WRCS, 2021). Hourly measurements of air temperature,

precipitation, wind speed, wind direction, and relative humidity were retrieved from the two stations within my study region, converted to daily average values, and formatted to match the standards required by SnowModel.

NOAA-CDO data from the Jackson Airport weather station were obtained using the CDO data retrieval tool. Daily measurements of air temperature, precipitation, wind speed, wind direction, and relative humidity were retrieved, converted to metric units where applicable, and formatted to the standards required by SnowModel.

The in-situ meteorological data was supplemented with data from CFSv2 - modeled reanalysis meteorological data sourced from the National Oceanic and Atmospheric Administration's (NOAA) National Centers for Environmental Prediction (NCEP) CFSv2 (Saha et al., 2011). CFSv2 data are modeled four times per day in 6-hour averages at a 0.2 arc-second spatial resolution and capture a range of variables including air temperature, precipitation, specific humidity, geopotential height, and v and u components of wind direction among many others. CFSv2 pixels were converted into "virtual" weather stations using *R's spatial* package, where the location of each "station" was taken as the centroid of the pixel and elevation was taken as a product of geopotential height at surface. This process effectively produced an ordered grid of weather stations across the study region where each daily measurement was taken at ground surface. Daily values of temperature, precipitation, wind speed, and wind direction were calculated as an average of the four measurements CFSv2 captures each day and relative humidity was computed using daily averaged specific humidity value, daily average temperature, and the Clausius-Clapeyron relation (Brown, 1951). Modeled precipitation inputs were also increased by 18.5% during SnowModel calibration as

CFSv2 precipitation has been shown to underestimate precipitation up to 20% (Yuan et al., 2011). Finally, all meteorological data were converted by station to the standards required by SnowModel and then combined into a single met file using SnowModel's included meteorological forcing pre-processing script.

Digital elevation maps and landcover data were retrieved using Google Earth Engine, a cloud-based and free-to-use GIS software. A digital elevation map of the region was retrieved from the Global Multi-resolution Terrain Elevation Dataset (GMTED) 2010 (Danielson & Gesch, 2010). GMTED is a product of NASA's Shuttle Radar Topography Mission (SRTM), which generated a digital elevation model of elevation data at a resolution of 1 arc-second. Landcover data was retrieved from the Copernicus Global Land Cover 2015-2019 dataset which classifies 23 different classes of landcover data at a 100m resolution (Buchhorn et al., 2020). Landcover data was reclassified to match the land classes recognized by SnowModel. Both raster layers were clipped to the study region, used at their native resolutions of 100m, and converted to ASCII using R *spatial* package.

#### *Snow-Water Equivalent Assimilation*

As an optional input, users can assimilate SWE, snow depth, and snow density observations to create a correction field that forces SnowModel inputs to match those observed in-situ at certain dates specified by the user (Liston & Elder, 2006). For the purposes of this study, correctly estimating peak SWE at the start of the ablation is imperative as too much snow or too little snow at the start of the snowmelt period can alter resulting calculations of peak SWE, total snow volume, and SDD. Snow-water

equivalent observations at the nine SNOTEL stations were assimilated on April 1<sup>st</sup> (the start of the ablation period) of each simulation year by first extracting observed SWE values from each station and formatting the data to match the standards required by SnowModel.

### *SnowModel Calibration*

A SnowModel run with the time-decay of snow albedo parameterizations from Gleason & Nolin (2016) (base model) was initialized to perform model calibration and to provide a base line from which to compare the postfire forest and postfire albedo models with. The parameterization from Gleason & Nolin (2016) originally used landcover class 5 to apply postfire albedo decay and albedo ranges to burn regions. For the purposes of creating a base model from which to compare the parameterizations used in this study, the Gleason & Nolin (2016) parameterization was modified such that no postfire parameterizations would be applied and landcover class 5 would follow snow albedo decay trends associated with an unburned forest.

Following these modifications, SnowModel was calibrated by running the base model iteratively using different sets of parameters and, following each run, modeled SWE values were compared with the time-series of observed SWE values obtained from the SNOTEL stations within the study region. For calibration purposes, four of the nine SNOTEL stations were excluded from the meteorological inputs to use as a validation-only set. Over the course of 21 model runs, the best calibration was found using the default parameters of SnowModel, but with the modeled precipitation inputs increased by 18.5%, an amount consistent with previous research from Yuan et al. (2011) that found

that CFSv2 modeled reanalysis data can underestimate precipitation results by up to 20% (Yuan et al., 2011).

Modeled values at the observation locations were extracted by locating the cell containing each SNOTEL station and the associated observed SWE measured by the SNOTEL station for that time step. Modeled SWE depth (SWED) was then compared to the observed SNOTEL measurements using four calibration statistics and thresholds outlined by watershed modeling from Moraisi et al (Moraisi et al., 2007). Pixel values were extracted using the *spatial* package within *R* and the performance statistics were calculated using the *HydroGOF* package. Following 21 calibration runs, ideal parameters were found that met the performance thresholds (Table 2). Values of these four statistics were averaged across each station for all snow seasons to produce performance metrics at each station. An overall calculation of model performance was computed by combining all SNOTEL data into a single dataset, combining all modeled data into a single data set, and then calculating the same performance metrics between the combined observed data and combined modeled data.

Four calibration statistics were calculated on the modeled SWED values: Root-Squared Error, Normalized Squared Error, R-squared, and Percent Bias. Root square error (RSR) is the root mean square error (RMSE) divided by the standard deviation. RMSE captures error or deviation from the observed value while division by the standard deviation normalizes the error so that the index can be applied and compared to variables of differing scales. Lower RSR is desired where zero RSR means the modeled results have perfectly matched the observed values. Following calibration, overall RSR was found to be  $RSR = 0.44$ , below the performance threshold of 0.70 (Table 2).

The Nash-Sutcliffe Efficiency (NSE) metric is a relative measure of the modeled residual variance compared to the variance in the observed data and indicates how well the plot of observed versus simulated data fits the 1:1 line (Nash & Sutcliffe, 1970; Moraisi et al., 2007). NSE has a range of  $-\infty$  to 1 with  $NSE = 1$  being the most optimum value. The performance threshold for NSE was  $NSE > 0.50$  and was met with an overall value of  $NSE = 0.81$  following calibration (Table 2).

The coefficient of determination ( $R^2$ ) describes the proportion of variance in the observed data explained by the modeled results and ranges from 0 to 1, with  $R^2 = 1$  meaning 100% of the variation in the observed data is explained by the model. A performance threshold of  $R^2 > 0.6$  was used for the calibration of SnowModel and was met with an overall value of  $R^2 = 0.85$  (Table 2).

Percent bias (PBIAS) is the tendency for the modeled results to under- or overestimate the observed results at a given timestep and can be either negative or positive, respectively. The optimal value of PBIAS is 0%, indicating that the modeled results do not under- or overestimate the observed data. A PBIAS threshold of  $PBIAS \leq |15\%|$  was used for calibration and was met with an overall final value of  $PBIAS = +11.40\%$  (Table 2).

Modeled results of SWED at the grid-cells associated with each of the SNOTEL stations were plotted over the entire study period to visualize the goodness of fit of the modeled results to the observed SWE. These results were plotted for all nine SNOTEL stations within the study area and a subset of these results are included here as an example (Figure 3). Post-calibration, SnowModel predicted the accumulation and ablation rates well, but showed a tendency to overestimate peak SWE by 11.40% across

all stations, a level of overestimation acceptable given the performance threshold ( $|\text{PBIAS}| < 15\%$ ) (Table 2).

*Parameterizations of postfire albedo decay, land cover change, and recovery*

Following calibration, I developed and incorporated postfire effect parameterizations of postfire effects on snow albedo, snow albedo decay, and forest structure over recovery into SnowModel. The modified snow albedo decay parameterizations were derived from the time-decay of snow albedo equation parameterized by Gleason et al. (2016) and the recovery was informed by the analysis of long-term postfire recovery of MODIS-retrieved surface snow albedo data by Gersh et al. (2022) (Gleason & Nolin, 2016; Gersh et al., 2022). Further information on the methods used to inform the model of long-term postfire recovery and the associated results can be found in Appendix A and Appendix B.

First, five albedo decay functions were computed by calculating five equally spaced exponential decay parameters between the postfire and unburned open albedo decay functions from Gleason and Nolin (Gleason & Nolin, 2016). This resulted in five unique albedo decay functions, each representing three years of recovery between the ignition date and the end of the 15-year recovery period. For example, the first equation represented postfire albedo decay from 1-3 years postfire, the second equation represented postfire albedo decay from 4-6 years postfire, and so on. In such a way, albedo decay was parameterized to return to the trends of an unburned open region by the 15<sup>th</sup> year following each burn's ignition year over five 3-year recovery steps (Figure 2).

A similar method was used to calculate and update the minimum and maximum albedo values over each period of recovery. Stepwise minimum and maximum albedo

values were computed by calculating five equally spaced steps between the post-burn minimum and maximum albedo and the unburned open minimum and maximum albedo (Gleason & Nolin, 2016). Like the albedo decay functions, each subsequent set of albedo minima and maxima represents the range of snow albedo of a burned region for each 3-year interval following ignition. For example, the first range of snow albedo values represented the snow albedo minimum and maximum of a postfire burn region 1-3 years postfire, the second range of snow albedo values represented the snow albedo minimum and maximum of a postfire region 4-6 years postfire, and so on. In such a way, snow albedo ranges returned to the snow albedo minimum and maximum of an unburned open region 15 years following ignition over five 3-year recovery steps.

The complete modified snow albedo decay parameterization solves for daily mean snow albedo using a time-varying exponential decay coefficient, where the degree of decay and the minimum and maximum snow albedo are modified by the number of periods since the burn event occurred. The recovery rates ( $\Delta K_a$ ,  $\Delta \alpha_{snow,min}$ , and  $\Delta \alpha_{snow,max}$ ) represent the five equally-spaced intervals of the decay coefficients and albedo minimum and maximum between the postfire burned forest snow albedo decay model and the unburned open meadow albedo decay model. By applying these recovery terms times the number of periods since burn to the associated variables ( $K_a$ ,  $\alpha_{snow,min}$ , and  $\alpha_{snow,max}$ ), the three values were “recovered” in a stepwise fashion back to snow albedo decay coefficients and snow albedo minimum and maximum of an unburned open meadow region over 15 years.

The parameterization operated by first resetting the snow albedo following a fresh snowfall event. For an unburned cell, the snow albedo value was reset to an associated,

unvarying maximum albedo based on the landcover type (forested or open). For a burned cell, snow albedo was similarly set to maximum burned snow albedo value, but in this case the value was modified as a function of number of periods following the initial burn (Equation 1).

$$\alpha_{snow} = \alpha_{snow,max} + (p * \Delta\alpha_{snow,max}) \quad (1)$$

In following time steps, unburned cells exponentially-decay as a function of daily time steps based on the coefficients determined by the landcover type. For a burned cell, snow albedo decayed using an exponential decay coefficient that was modified by the number of periods (3-year intervals) since the fire occurred (Equation 2). During this step, minimum burned snow albedo values were also updated in a similar fashion.

$$\begin{aligned} (\alpha_{snow})^{n+1} = & (\alpha_{snow,min} + \Delta\alpha_{snow,min} * p) \\ & + ((\alpha_{snow})^n - (\alpha_{snow,min} + \Delta\alpha_{snow,min} * p))^{[-K_{\alpha} + \Delta K_{\alpha} * p] * dt} \quad (2) \end{aligned}$$

Finally, forest structure was parameterized by calculating five equally spaced snow-holding depth (SHD) values between that of a scattered conifer forest (simulating forest structure in an immediate postfire state) and that of an open meadow. The SHD value is used in SnowModel to calculate the snow holding capacity of vegetation within each grid cell. The snow depth of a cell must exceed this value before snow can reach the ground and become available for wind redistribution and be subjected to wind ablation effects and canopy-modified solar forcing. To simulate a “recovery” of land cover change from burned forest to an open meadow, the associated snow-holding depths (SHD) were

modified in a stepwise fashion from values of a scattered conifer forest to those of a sparse, open region using the default values from those land classes included in SnowModel (Equation 3).

$$SHD_{burn} = SHD_{forest} - (\Delta SHD * p) \quad (3)$$

Similar to the snow albedo parameterizations, these SHDs are updated over 5 equally spaced intervals as a function of periods since the burn occurred.

Ideally and intuitively, albedo decay coefficients, albedo snow albedo minima and maxima, and SHD values would be updated on an annual basis, but this was not possible with the current iteration of SnowModel. Five steps were utilized due to a limitation in SnowModel that only allows 5 custom classes to be created by the user and, because five equally spaced steps were used, the albedo decay equations and snow albedo minimum and maximum shift one step closer to an open region every three years following fire. The three years within each period essentially operate off the same snow albedo decay coefficients and snow albedo minimum and maximum and this is reflected in the period-wise analysis methods to follow.

Using these parameterizations, two parameterized models were created: a postfire forest model and a postfire albedo model. The postfire forest model used only the postfire effects on forest structure and recovery parameterization (equation 3) simulating only the postfire effects on forest structure and associated recovery with no parameterizations for postfire effects on snow albedo or recovery included. The postfire albedo model used all three parameterizations (equations 1-3) and simulated both the postfire effects on snow albedo and forest structure and the associated recovery of each over 15 years postfire.

Using a model that combined both the postfire effects on forest structure and snow albedo (postfire albedo model) along with a model that incorporated only the postfire effects on forest structure allowed for compartmentalization of postfire effects on snow hydrology due to forest structure from postfire effects on snow hydrology due to postfire effects on snow albedo.

### *SnowModel Batch Runs*

To apply the correct snow albedo decay equations, snow albedo minimum and maximum, and forest structure to each burn at the correct time, I utilized reclassified land cover rasters over 20 1-year “batch” runs of SnowModel. Annual landcover rasters were created by reclassifying burn areas in the vegetation input of SnowModel with values corresponding to each fires’ period of recovery over time. The landcover input was brought into *R* and, using the *spatial* package, pixels within the MTBS burn regions were reclassified with the custom class corresponding to each fires’ period of recovery over time. At ignition date and every subsequent three years postfire, the pixels within a respective burn region were set to a custom landcover class which was used to determine which set of snow albedo decay equations, snow albedo minimum and maximum, and SHDs for SnowModel to use in the energy balance equations. Fifteen years after ignition, the landcover values were set to a standard landcover class corresponding to an open meadow. At this point, cells within the burn region followed the standard equations for an open region. Because SnowModel does not support multiple landcover rasters for a single run, I developed an automated batch method wherein SnowModel runs in one-year increments, each time selecting the appropriate landcover raster, meteorological forcing data, and SWE assimilation date for that year. Following each run, SnowModel outputs

were converted from the native GrADs format to netCDF for later processing and analysis using *R*.

*Analysis of Model Results: Snow Volume and Disappearance Date Calculations*

Following the parameterized (postfire forest and postfire albedo) batch runs, SnowModel outputs for the postfire albedo model and base model were differenced and compared for changes in peak SWE and total SWE and SDD shifts due to parameterization of postfire effects. All calculations were performed within *R* using the *spatial* package.

Postfire impacts were quantified by subtracting the base model results from the corresponding rasters from the same time-step of the postfire albedo model results. This produced differenced rasters which isolated the change in SWE due to postfire effect and recovery parameterization. The differenced SWE values from within the burn regions were then isolated using MTBS burn boundaries. Calculations were then performed in each burn region to determine changes in total SWE immediately following fire, changes in total SWE over the full recovery period, changes in peak SWE averaged over each recovery period, and changes in SDD averaged over each recovery period.

Change in total SWE immediately following fire was quantified by identifying the date of peak SWE for the first year following fire for the base and postfire albedo models. Peak SWE date for each year was defined as the date of the maximum average SWE of all pixels within each burn region for the year in question. Once the date of peak SWE for the base and postfire albedo models were identified, the two associated modeled rasters were differenced and the SWE depth values of each pixel within each burn region were converted from measurements of SWE depth to measurements of SWE volume by

multiplying the SWE depth values (in meters) by  $100^2$  (the spatial resolution of the modeled rasters was  $100 \text{ m}^2$ ) to produce a change in total SWE due to postfire effects. Changes in total SWE over the full recovery period were calculated by performing the above calculation for every year following the ignition date of each burn and summing the results over the entire postfire period.

Changes in peak SWE and SDD over postfire recovery were calculated as averages over each 3-year period following fire. Due to the albedo decay and landcover parameterization only changing every 3 years following fire, values were averaged in three-year periods to produce a maximum of five total period-average peak SWE differences and associated standard deviations, as well as SDD shift values due to postfire effects for each fire. In this way, each calculation represents an average change in peak SWE or average shift in SDD over each 3-year recovery period due to postfire effects. A postfire recovery calculation was also computed using the model results for the 16<sup>th</sup> year following fire when albedo decay, albedo minimum and maximum, and forest structure had fully recovered to an unburned, open state. Most burns occurred later than 5 years into the 20-year modeling period and in these burns period-wise change in peak SWE and SDD were calculated for only the periods of available data. In the case of burns with less than 3 years of data available for their final modeled period, an average of the data that was available was calculated. In the case of burns where only one year of data was available for the period, the period calculation represents only a single, unaveraged date and thus no standard deviation was calculated.

Period-wise change in total SWE was calculated for each fire as a measure of how snow volume is affected by postfire impacts and recovery over time and was calculated

by averaging the total volumetric change in SWE (again, converting the modeled SWE depth values to volumetric SWE) at time of peak SWE over each recovery period following ignition date. Postfire shift in SDD was calculated for each period to provide a measure of how snowmelt timing is affected by postfire effects and how these shifts change over the course of recovery. For each burn region, SDD was defined as the first five-day period where no snow cover was observed within the burn region with the SDD centered on the middle of that same period. Snow disappearance date was calculated for each burn in each of the years following ignition date. Annual dates of snow disappearance for each burn were then converted to Julian day using the *lubridate* package in *R* and the resulting values from the base model were differenced from the postfire albedo model. This produced an annual shift in SDD for every fire for each year following ignition date. The results were then averaged in 3-year bins to produce a final value of average shift in SDD and standard deviation of SDD shift among the three years for each three-year recovery period following each burn.

*Analysis of Model Results: Spatial and Daily Variability of SWE over Season and Recovery*

Spatial variability of changes in SWE over the snow season was visualized to analyze how postfire effects on snow albedo and forest structure affect snow distribution, both seasonally and over long-term recovery. Changes in SWE over the snow season were visualized by differencing the postfire albedo and base model rasters of March 1<sup>st</sup> (accumulation), April 1<sup>st</sup> (start of ablation), and May 1<sup>st</sup> (ablation) to produce a three change in SWE rasters for each date and each year for each fire. The differenced rasters were then averaged over each 3-year recovery period (like the methods used in period-

wise change in peak SWE and SDD shift), effectively producing a period-averaged March 1<sup>st</sup>, April 1<sup>st</sup>, and May 1<sup>st</sup> differenced raster for each recovery period. The average proportional change in SWE and 95% confidence interval were also calculated and annotated on each plot. All calculations were computed in *R* using the *spatial* package.

Daily SWE depth plots were created for each burn over the recovery period to highlight differences in how snow accumulates and melts in forests affected by wildfire over recovery. For each burn, SWE depth values in each pixel were averaged for each daily time-step for all three models. These values were then averaged over period to produce period-averaged SWE for each day of the water year for each recovery period.

#### *Quantification of Watershed Scale Impacts*

Watershed scale impacts of postfire effects and recovery were investigated within the Lower Granite Creek HUC12 subbasin. A United States Geological Survey (USGS) delineation of the watershed was extracted using the Living Atlas tool in ArcGIS and exported into *R* (USGS, 2019). Modeled SWED rasters over the 20-year period for both the base model and postfire albedo model were clipped with the watershed delineation file using the *spatial* package in *R*. Corresponding May 1<sup>st</sup> SWE depth within the watershed were differenced between the base and postfire albedo models and plotted in a matrix, with each image overlaid on a hill shade DEM of the surrounding area. Using *R*, the proportional difference in SWE within the watershed between both models was calculated. Total SWE difference over 20 years between both models was summed and the total volume of snow difference was calculated as well as the proportional difference and 95% confidence interval (annotated on each subplot). Finally, the percentage of

watershed burned for each of the three fires occurring within the basin was calculated using the Calculate Shape Area tool in ArcGIS.

### *Statistical Analysis*

Differences between the base model and postfire albedo model results were tested for statistical significance using a two-sided, two-sample Welch t-test using an alpha value of 0.05. I tested for statistically significant differences between the base model and postfire albedo model for the following metrics: immediate peak SWE change, total peak SWE change 1-15 years postfire, period averaged peak SWE changes, and period averaged change in SWE rasters. All results were analyzed for statistical significance by selecting 100 random pixels within each burn region from the corresponding base model and postfire model rasters and running the t-test using base functions and the *raster* package within *R*.

For immediate peak SWE change, the date of peak SWE for the first year following fire was found by calculating average SWE within each burn region during the first year following fire for both the base model and postfire, 100 random pixel values of SWE were selected from within each burn regions for each of the models, and set of modeled SWE values were tested for significant differences.

For total peak SWE changes, the date of peak SWE was found for every year following fire for both the base model and postfire albedo model and the rasters were summed using the *spatial* package within *R* to produce a stack of peak SWE rasters including every year since fire. Again, 100 random pixel values of SWE were selected from each raster from within each of the burn regions and the resulting modeled SWE values were tested for significant differences using a t-test.

Period averaged peak SWE changes were tested for significant differences in a similar fashion, except rather than calculating summed rasters of peak SWE over the entire postfire period for each fire, postfire peak SWE rasters were averaged in 3-year bins following the ignition date. Random samples of 100 pixel values of SWE from within the burn regions of the corresponding averaged 3-date peak SWE stacks of the base model and postfire albedo model were then extracted and tested for significant differences using a t-test.

Finally, to test for significant differences between period averaged March 1<sup>st</sup>, April 1<sup>st</sup>, and May 1<sup>st</sup> results, the three dates were selected from each year following fire and averaged in 3-year bins following ignition date. Random samples of 100 pixel values of SWE were then extracted from the period-averaged rasters from within each burn region and the two sets of modeled SWE values were tested for significance using a t-test. All figures and tables including metrics tested for significance show asterisks denoting the level of significance found for each of the tests, but p-values calculated for each test can also be found on Table A3 in the Appendix Figures and Tables section.

### *Model Validation*

Modeled SWE outputs from the base model and postfire albedo model were validated using field measurements of SWE taken from six of the modeled burns (Horsethief Canyon, Bull, Boulder, Cliff Creek, Lava Mountain, and Roosevelt) during February and March of 2019 (Figure 1). These measurements have not yet been published and were made available through the Portland State University Snow Hydrology lab via Dr. Kelly Gleason. Prior to validation, the field data were preprocessed using *R*. Originally, the 114 SWE measurements were collected inside and outside the

burn so I first subset the measurements based on measurements that fell within the MTBS burn boundaries of each of the six fires. At each site within the burns, one to three replicates of SWE measurements were taken and, due to the close proximity of the replicates and the modeling resolution of 100 m<sup>2</sup>, replicates were averaged as they always fell within the same modeled pixel. Average measured values were then matched with corresponding modeled SWE results from the base model and postfire albedo model using their geographic coordinates and date of collection and the average percentage difference between the values were computed for each fire. In addition, an overall average percentage difference was calculated by computing average percentage difference between all observed measurements and the associated base model SWE and postfire albedo model SWE.

## RESULTS

Postfire reductions in albedo and forest cover decreased snow volume and shifted SDD earlier persistently for up to 15 years following the initial ignition date (Table 3). Post-recovery (>15 years postfire), two burns still showed altered peak SWE and SDDs (Table 3). While snow accumulation increased slightly during the accumulation period (March 1<sup>st</sup>), additional melting caused by increased solar forcing from canopy loss and reductions albedo were persistent throughout the 15-year recovery period (Figures 4-11). This resulted in additional melting relative to the base model throughout each snow season following fire, leading to reduced peak snow volume and earlier SDDs relative to the pre-fire level (Table 3).

### *Immediate Postfire Effects on Snow Volume and Snow Disappearance Date*

The greatest reductions in snow volume and shifts in SDD generally occurred in the winters immediately following ignition (1-year postfire). Relative to the base model, the postfire albedo model showed decreases in peak SWE volume of between 485K m<sup>3</sup> and 10M m<sup>3</sup>, proportional losses in peak SWE of between 2.81% and 31.91% (Table 3: Immediate Peak SWE Loss [ $<1$  YPF]), and earlier SDDs of between 33 to 58 days (Table 3: SDD Shift Averaged Over Period 1). A larger burn area typically resulted in greater losses in snow volume, while burns of smaller area resulted in the lowest losses in snow volume. The two largest burns, the Roosevelt (224 km<sup>2</sup>) and Cliff Creek (146 km<sup>2</sup>) (Table 3: Elevation), caused the greatest losses in snow volume in the year immediately following ignition (10.60M m<sup>3</sup>;  $p < 0.01$  and 7.89M m<sup>3</sup>;  $p < 0.001$ ) (Table 3: Immediate Peak SWE Loss [ $<1$  YPF]). The Boulder and Green Knoll burns (15 km<sup>2</sup>) showed the

lowest losses of 804K m<sup>3</sup> (p < 0.001) and 474K m<sup>3</sup> (p < 0.001), respectively (Table 3: Immediate Peak SWE Loss [ $<1$  YPF]).

Trends of increasing SWE loss with increasing burn area were not entirely consistent, however. The smallest modeled burn, Horsethief Canyon (11 km<sup>2</sup>), caused losses of 1.87M m<sup>3</sup> (p < 0.001) of snow volume – volumetric losses 2.45 and 3.86 times greater than the losses caused by the larger burns of Boulder (764K m<sup>3</sup>; p < 0.01; 15 km<sup>2</sup>) and Green Knoll (484K m<sup>3</sup>; p < 0.05; 15 km<sup>2</sup>) – and the greatest proportional loss in peak SWE (31.91%; p < 0.001) of all burns 1-year postfire. Similarly, the Lava Mountain burn caused immediate (1-year postfire) volumetric and proportional losses in snow volume on par or greater than those caused by the Cliff Creek burn (7.82M m<sup>3</sup>/17.05%/p < 0.001 vs. 7.88M m<sup>3</sup>/8.82%/p < 0.001) despite burning 60% less area (59 km<sup>2</sup> vs. 146 km<sup>2</sup>). While greater burn area did often result in greater volumetric losses of SWE immediately following burn, burn size alone did not explain the impacts on resulting loss in snow volume (Table 3).

#### *Immediate Postfire Effects on Seasonal Snow-Water Equivalent*

Immediate postfire effects on seasonal SWE were analyzed as modeled results averaged over the first recovery period (1-3 years postfire) or “period 1”. Seasonal trends in postfire effects on snow highlight why the size of a burn did not always predict how severe the immediate postfire impacts would be. Analysis of the spatial and seasonal variability in SWE difference caused by postfire effects showed altered snowpack evolution during accumulation, start of ablation, and ablation. March 1<sup>st</sup>, April 1<sup>st</sup>, and May 1<sup>st</sup> were selected as the dates for accumulation, start of ablation and ablation respectively and these dates were analyzed for spatial and seasonal differences in SWE

caused by postfire effect and recovery parameterizations (Figures 4-11). In general, the direction and magnitude of changes in SWE due to postfire effects corresponded with the relative elevations where each burn occurred. High elevation burns tended to have higher accumulation rates immediately following ignition, while lower elevation showed losses as early as the accumulation period (Table 3). Immediate postfire effects caused reductions in SWE at all but the highest elevation burns start of ablation and all fires showed substantial losses by the ablation season (Table 3).

During accumulation of recovery period 1, SWE increased slightly due to the reduced canopy cover present burned regions. The postfire albedo model and postfire forest model followed similar accumulation trends (Figures 4d-11d: Period 1) throughout recovery period 1 and SWE accumulation was greater than the base model. Across the burn area, SWE accumulation was generally greater in the postfire recovery model during recovery period 1. The Roosevelt (Figure 5a: Period 1;  $p < 0.05$ ), Bull (Figure 7a: Period 1;  $p < 0.001$ ), Cliff Creek (Figure 8a: Period 1;  $p > 0.05$ ), Lava Mountain (Figure 10a: Period 1;  $p > 0.05$ ), and Purdy (Figure 11a: Period 1;  $p < 0.001$ ) burns all showed greater average SWE during the accumulation season 1-3 years postfire ( $+4.25\% \pm 3.01\%$  to  $+6.93\% \pm 1.21\%$ ). In contrast, postfire effects in the Boulder (Figure 6a: Period 1), Green Knoll (Figure 4a: Period 1) and Horsethief Canyon (Figure 9a: Period 1) burns all caused significant losses ( $p < 0.001$ ) in accumulation SWE during recovery period 1 ( $0.46\% \pm 3.48\%$  to  $3.64\% \pm 1.81\%$  reduction). The Green Knoll and Horsethief Canyon burns occurred at the lowest elevations on average (2168m and 2281m) (Table 3) and period 1 accumulation losses were likely driven by the reductions in albedo combined with warmer temperatures at lower elevation. Snowpack at lower elevations is relatively

warmer on average than high elevation snowpack, resulting in earlier melting outcompeting the increased accumulation caused by reduced canopy cover (Lundquist et al., 2013).

Losses in SWE began to manifest immediately following fire (period 1) during start of ablation (April 1<sup>st</sup>) across all modeled burns. Burns at low elevation showed greater SWE losses on average while higher elevation burns (elevation > 2300 meters) showed decreased losses or even slight gains in April 1<sup>st</sup> SWE over recovery period 1. The Green Knoll burn, (average elevation = 2168m), showed a  $29.12\% \pm 71.64\%$  ( $p < 0.001$ ) reduction in average April 1<sup>st</sup> SWE during recovery period 1 due to postfire effects (Figure 4b: Period 1). In contrast, the Lava Mountain burn, with an average elevation of 2565m, showed only slight losses in average April 1<sup>st</sup> SWE ( $-2.1\% \pm 13.95\%$ ;  $p < 0.001$ ) during recovery period 1 (Figure 10b: Period 1). The Purdy event, the highest elevation burned forest on average (2740m), showed slight gains in April 1<sup>st</sup> SWE ( $+2.17\% \pm 6.69\%$ ;  $p < 0.001$ ) during recovery period 1 (Figure 11b: Period 1). In general, 1-3 years following fire postfire effects caused the greatest losses in April 1<sup>st</sup> SWE in fires occurring at lower elevation and decreased losses or gains in April 1<sup>st</sup> SWE in fires occurring at higher elevation. It is likely that warmer temperatures at lower elevation drove greater losses in peak SWE relative to the higher elevation burns.

One to three years following fire (period 1), postfire effects on snow caused losses in SWE during the ablation (May 1<sup>st</sup>) season and these losses were greater than those observed during start of ablation (April 1<sup>st</sup>). Less snowfall during ablation meant that albedo decayed further, resulting in additional solar forcing on snow and overall warmer, riper snowpack more prone to melting. Much of the gains in March 1<sup>st</sup> SWE during

recovery period 1 were counteracted by losses during the ablative seasons, resulting in a net reduction in snowpack by the ablation season (May 1<sup>st</sup>). All fires showed only decreases in May 1<sup>st</sup> SWE during recovery period 1 with the greatest proportional losses occurring in the Boulder (-87.97%  $\pm$  7.98%;  $p < 0.001$ ) and Green Knoll (-76.63%  $\pm$  26.47%;  $p < 0.001$ ) fires (Figure 6c: Period 1 and Figure 4c: Period 1). The Cliff Creek Fire, a burn which showed gains in March 1<sup>st</sup> snow volume (+4.58%  $\pm$  1.72%;  $p > 0.05$ ) during recovery period 1 (Figure 8a: Period 1), showed substantial period 1 May 1<sup>st</sup> losses (-47.26%  $\pm$  40.96%;  $p < 0.001$ ) with all areas of prior increases in period 1 March 1<sup>st</sup> SWE showing declines by period 1 May 1<sup>st</sup> (Figure 8c: Period 1). A similar effect was observed in the Roosevelt burn where modest gains in snow volume during March 1<sup>st</sup> period 1 (+6.93%  $\pm$  1.21%;  $p < 0.05$ ) and April 1<sup>st</sup> period 1 (+0.10%  $\pm$  3.15%;  $p > 0.05$ ) shifted to significant declines by May 1<sup>st</sup> period 1 (-45.76%  $\pm$  3.15%;  $p < 0.001$ ) (Figures 5a-c: Period 1). The only exception was in the Purdy burn, which showed small increases in SWE at high elevation during May 1<sup>st</sup> period 1 (Figure 11c: Period 1), although these increases were reduced from the previous gains observed at April 1<sup>st</sup> period 1 (Figure 11b: Period 1) with an overall average loss in SWE (shift from +2.17  $\pm$  6.69%;  $p < 0.001$  to -9.93%  $\pm$  36.85%;  $p > 0.05$ ) (Figure 11c: Period 1).

#### *Postfire Effects on Snow Volume and Snow Disappearance Date over Recovery*

Following the immediate postfire period, snow volume, peak SWE and SDD in the postfire albedo model began to approach values more similar to the base model as snow albedo and decay recovered from an immediate postfire state towards an unburned open meadow. However, the shift in forest structure and albedo decay of a sparsely forested postfire state towards those of a post-recovery open canopy state parameterized

in the postfire albedo and postfire forest models still resulted in differences in snow hydrology relative to the base model beyond the 15-year recovery period.

In the burns modeled for up to 15 years postfire (Boulder and Green Knoll), the greatest losses in volumetric peak SWE did not occur 1-3 years following fire (period 1), but instead 4-9 years postfire (periods 2 and 3). Volumetric and proportional SWE losses in these burns tended to increase in magnitude 1 to 9 years postfire and then decrease in magnitude 10+ years postfire (Table 3; Boulder, Green Knoll, and Purdy). For instance, postfire effects on snow albedo and forest structure in the Boulder burn region caused the greatest loss in peak SWE (-1.1M m<sup>3</sup>/SD: 454K m<sup>3</sup>; -11.81%/SD: 3.12%; p < 0.001) 7-9 years postfire (Table 3: Boulder - Period 3), while the greatest peak SWE losses in Green Knoll and Purdy fire (-1.9M m<sup>3</sup>/SD: 621K m<sup>3</sup>; -26.02%/SD: 10.17%; p < 0.001 and -4.7M m<sup>3</sup>/SD: 412K m<sup>3</sup>; -8.89%/SD: 1.09%; p < 0.01) occurred 4-6 years postfire (Table 3: Green Knoll – Period 2 and Purdy – Period 2).

Shifts in SDD were greatest immediately following fire and smallest 16 years postfire (Table 3: SDD Shift Averaged Over Period). However, shifts in SDD did not decrease in magnitude consistently over the course of postfire recovery. In the case of the Boulder fire, SDD shifts increased in magnitude 7-12 years postfire where snow disappeared later on average during years 10-12 than during years 7-9 (period 3: -30 days/SD: 2 days to period 4: -31 days/SD: 2 days) (Table 3). Snow disappearance within the Green Knoll burn region showed similar trends with snow disappearing later, on average, 7-9 years postfire (period 3: -34 days/SD: 8 days) than it did 4-6 years postfire (period 2: -27 days/SD: 4 days) (Table 3). Although shifts in SDD tended to decrease

progressively over the course of postfire recovery, the recovery of snow retention was not consistent over years since fire, and SDD shifts advanced yet again 4-12 years postfire.

Losses in peak SWE over postfire recovery tended to decline 4 to 9+ years following fire yet impacts on snow hydrology still persisted 15+ years following fire when postfire effects on snow albedo had subsided. Peak SWE within the Boulder burn region increased significantly by 2.32% (196K m<sup>3</sup>;  $p < 0.001$ ) 16 years postfire. Conversely, postfire effects in the Green Knoll burn region caused a 2.20% reduction peak SWE 16 following fire (-241,246 m<sup>3</sup>;  $p < 0.001$ ). Similarly, SDD in the postfire albedo model still showed changes relative to the base model 16 years postfire. Snow disappeared in the Boulder burn region 2 days earlier than in the base model 16 years postfire and, in the Green Knoll burn region, snow disappeared 6 days later (Table 3: SDD Shift Averaged Over Period). Together, the lasting postfire impacts on peak SWE and SDD indicate that even after postfire effects on snow albedo have dissipated 16 years following fire, the shift in landcover from forest to an open meadow can still result in lasting impacts on snow hydrology beyond the 15-year postfire recovery period.

#### *Recovery of Postfire Effects on Seasonal Snow-Water Equivalent*

Over the 15-year postfire recovery of each fire, increases in accumulation were generally found to increase over each successive recovery period. For example, average SWE during accumulation (March 1<sup>st</sup>) within the Bull burn region increased in magnitude and extent over the four recovery periods modeled (period 1: +2.61% ± 16.99%,  $p < 0.001$ ; period 2: +1.53% ± 4.07%,  $p < 0.001$ ; period 3: +0.70% ± 1.19%,  $p > 0.05$ ; period 4: +3.38%,  $p < 0.001$ ) (Figure 7a: Periods 1-4). Average SWE also increased over successive recovery periods in the Cliff Creek burn region (period 1: +4.58%; period 2:

+7.09%) and the Lava Mountain burn region (period 1: +4.29%; period 2: +11.57%) (Figure 8a and Figure 10a). However, this trend was not consistent across all burns. For instance, average March 1<sup>st</sup> SWE in the Green Knoll burn region decreased by 1.40% during 10-12 years postfire (period 4 of recovery) when the previous two years showed widespread increases in SWE accumulation (period 3: +7.13%; period 4: +5.43%) (Figure 4a).

Broadly, burns occurring at lower elevation showed greater losses on April 1<sup>st</sup> and slower recovery overall, while burns occurring at higher elevation showed immediate gains in April 1<sup>st</sup> SWE at their highest points of elevation and these gains continued to increase in magnitude and extent over the course of postfire recovery. Postfire reductions in start of ablation (April 1<sup>st</sup>) SWE then declined in magnitude over recovery in the years following fire. Lower elevation burns experienced gains in April 1<sup>st</sup> SWE in some locations starting in period 3 (7-9 years postfire) with SWE gains becoming more widespread and increasing in magnitude thereafter. For instance, the Green Knoll and Horsethief Canyon burns (the two lowest average elevation burns) showed widespread losses until period 3 of recovery when some increases in April 1<sup>st</sup> SWE occurred in some locations of the burn region (Figure 4b and Figure 9b). Burns occurring at higher elevation experienced April 1<sup>st</sup> SWE gains even earlier. The Purdy burn (elevation = 2740m) showed increases in April 1<sup>st</sup> SWE during every recovery period and these gains increased in magnitude by the final modeled period of recovery (period 1: +2.17%; period 5: +6.87%) (Figure 11b). Similar trends were found with other high elevation burns, such as the Lava Mountain and Bull burns which increased from -2.11% to +10.53% and -8.29% to +3.38%, respectively (Figure 10b and Figure 7b).

Postfire reductions in ablation season (May 1<sup>st</sup>) SWE declined over time following fire, but these changes were consistently negative throughout the entire recovery period for nearly every fire modeled (Figures 4c-11c). For instance, the two burn regions that were modeled for the entire recovery period (Green Knoll and Boulder) showed losses in May 1<sup>st</sup> SWE for every postfire recovery period. The Green Knoll fire shifted from average period 1 May 1<sup>st</sup> SWE losses of 76.63% immediately following fire to losses of 13.50% in the post-recovery period (Figure 4c) while the Boulder fire recovered from losses of 87.97% period 1 May 1<sup>st</sup> SWE to losses of 8.25% in the post-recovery (>15 years postfire) period (Figure 6c). Losses in May 1<sup>st</sup> SWE beyond period 5 indicate that even after snow albedo impacts have dissipated, losses in SWE still occur and this is likely due to the lasting post-recovery (15+ years postfire) change in forest structure caused by wildfire.

#### *Effects of Postfire Impacts and Recovery on Total Snow Volume*

Postfire effects on snow albedo and forest structure caused losses in total snow volume many times greater than the initial losses when annual losses were summed over the entire recovery period. Postfire effects on snow in the Boulder and Green Knoll burn regions (the two burns modeled for the entire 15-year recovery period) caused total losses of 5.53M m<sup>3</sup> (-3.83%) and 8.86M m<sup>3</sup> (-7.51%) of SWE (Table 3). While the other six burns were not modeled fully over their entire respective recovery periods, total losses were often far greater than the immediate losses alone. The Horsethief Canyon fire caused immediate losses of 1.18M m<sup>3</sup> which grew to total losses of 7.73M m<sup>3</sup> over 8 years of postfire recovery, a total loss 4x greater than the peak SWE losses in the year immediately following fire. Similarly, SWE losses caused by the Bull fire increased from

immediate postfire losses of 1.18M m<sup>3</sup> to total losses of 19.03M m<sup>3</sup>, an increase of over 17 times the immediate losses over 10 years of recovery (Table 3).

When proportional peak SWE losses were averaged annually over the recovery period, losses were greatest in the fires occurring at the lowest elevation, while the highest elevation burns experienced the smallest losses (Table 4). The lowest elevation burn, the Green Knoll fire, showed a 7.2% average annual decrease in peak SWE over the modeling period, while the highest elevation fire, the Purdy fire, only showed a 0.5% average annual loss (Table 4).

#### *Effects of Postfire Impacts and Recovery at the Watershed Scale*

Postfire effects on snow albedo and forest structure caused long-lasting and persistent reductions in May 1<sup>st</sup> SWE at the watershed scale. Three of the modeled burns (Boulder, Bull, and Roosevelt) occurred entirely or partially within the Lower Granite Creek (LGC) subbasin. The Boulder burn was the earliest occurring burn of all modeled burns (2000) and burned entirely within the LGC subbasin (15 km<sup>2</sup>; 13.05% of the watershed area), while the Bull and Roosevelt fires occurred partially within the LGC subbasin (burning 12 km<sup>2</sup> [10.48%] and 23 km<sup>2</sup> [19.81%] of the basin, respectively) (Figure 12). In combination, all three fires burned 43.37% of the watershed area over the 20-year modeling period (50.45 km<sup>2</sup>) making the LGC subbasin a useful representation of the watershed scale impacts of postfire effects and recovery on May 1<sup>st</sup> snow volume (Figure 12).

The burns occurring within LGC subbasin caused mostly annual losses in ablation season snow volume over 20 years ( $-6.30 \pm 6.95\%$  loss in May 1<sup>st</sup> SWE) with all years other than 2011 showing a net average loss in May 1<sup>st</sup> SWE (Figure 12). Postfire effects

on snow albedo and forest structure caused the greatest proportional losses in SWE during 2015 and 2019 (-9.50% and -14.58%). During 2015, postfire effects from both the Boulder and Bull fires impacted snow volumes within the LGC subbasin. The Bull fire occurred 5 years prior, and the Boulder fire occurred 15 years prior and, combined, the burns caused a 9.50% reduction in May 1<sup>st</sup> SWE. During 2019, postfire impacts from the Cliff Creek burn (occurring 3 years prior) caused a -14.58% reduction in May 1<sup>st</sup> SWE in combination with the postfire recovery effects from the Bull fire (occurring 9 years prior) (Figure 12; 2012 and 2019). Burns relatively late in their postfire recovery period continued to cause losses and enhanced immediate losses from more recent burns. Repeated burns within the LGC subbasin and the associated postfire impacts on snow and forest structure resulted in a total reduction of 5.85% in May 1<sup>st</sup> SWE over the 20-year modeling period, a total volume of >94M m<sup>3</sup> of additional snowmelt by May 1<sup>st</sup> (Figure 12).

#### *Model Validation*

The base model and parameterized model results were validated using field measured values of SWE taken from six of the modeled burns between February 9<sup>th</sup> and March 19<sup>th</sup> of 2019 and the percentage difference between the observed and modeled values for each of the six fires and all fires overall were computed (Table 5). Modeled SWE results from the base model and postfire albedo model were proportionally greater than the observed SWE values across all burns and overall indicating that both models overestimated SWE on average. Overall, the base model performed better in across all six burns where measured values were available (base: +40.22 ± 38.88% vs. postfire albedo model: +41.61 ± 46.29%). SWE in the postfire albedo model was closer to the observed values on average relative to the base model in three fires (Horsethief Canyon: +58.64%

vs. +61.06%, Bull:  $+23.03 \pm 33.79\%$  vs.  $+24.67 \pm 33.24\%$ , and Lava Mountain:  $+46.18 \pm 30.25\%$  vs.  $+48.89 \pm 24.08\%$ ), while the base model performed better in the other three fires (Boulder:  $+40.71 \pm 22.03\%$  vs.  $+41.22 \pm 22.3\%$ , Cliff Creek:  $+40.4 \pm 26.93\%$  vs.  $+41.17 \pm 19.53\%$ , Roosevelt:  $+59.79 \pm 26.84\%$  vs.  $+67.89 \pm 23.91\%$ ) (Table 5). The tendency for modeled results to overestimate the observed SWE indicates that the postfire albedo model and base model were likely underestimating postfire effects on snow in the locations where observed data were collected. Further, all field measurements were collected during the accumulation season between February 9<sup>th</sup> and March 19<sup>th</sup>, meaning that modeled results tended to overestimate observed SWE during periods of net negative snowpack energy balance. The base and postfire albedo model results tended to differ more during the ablation period, which explains why the percentage differences between the observed and base model and observed and postfire albedo model tended to be similar to one another. However, the observed data set was of a small sample size and the measurements were taken within a short time frame and within close proximity to one another (Figure 1). Conversely, the modeled results extend over many years and cover much larger areas and thus it is likely this data alone is insufficient to validate the modeled results.

## DISCUSSION

Forest fires in the seasonal snow zone accelerated snowmelt through the addition of black carbon into the snowpack and through modification of forest structure, effects which lasted for many years following ignition. Immediately following fire, snowpack within burned forests attained lower peak SWE and melted earlier, resulting in reductions in remaining snow volume by the ablation season. Over 15 years of postfire recovery, peak SWE and SDDs progressed towards base model levels as snow albedo and accelerated snow albedo decay rates shifted to levels of an unburned open meadow, but losses in peak SWE and earlier snowmelt were persistent throughout the entire postfire recovery period and beyond 15 years following fire. Landcover shifts from pre-fire forest to open meadow over 15 years postfire likely caused additional solar forcing on snow and wind ablation losses, resulting in reductions in peak SWE beyond the 15-year postfire recovery period. In total, persistent postfire effects on snow albedo and forest structure over 15 years following fire caused cumulative losses in peak SWE and resulting snow volume 8 to 17 times greater than the losses observed in the snow season immediately following ignition (Boulder and Green Knoll fires). At the watershed scale, watersheds burned for less than half of their area showed average annual reductions between  $1.14\% \pm 21.2\%$  to  $14.58\% \pm 76.1\%$  and an average annual reduction of  $6.30 \pm 6.95\%$  in ablation season snow volume over 20 years (Figure 12). Volumetric losses in snow volume due to postfire effects on snow summed over 20 years resulted in a total loss of  $>94\text{M m}^3$  (5.85%) in ablation season SWE (Figure 12).

### *Postfire Forest Structure Impacts on Snow Hydrology*

The degradation of forest structure due to wildfire enhanced accumulation rates relative to a densely forested, pre-fire state, but also resulted in increased solar forcing on the surface of snowpack and greater losses from wind ablation. The interplay between these two competing effects can result in varying effects on snowpack depending on the local climate (Essery et al., 2008; Musselman et al., 2008; Roth and Nolin, 2017). Over 15 years following fire, removal of canopy likely produced small increases in snow volume ( $+0.70\% \pm 1.19\%$  to  $+11.57\%$ ) during March 1<sup>st</sup>, with increased exposure to incoming shortwave radiation and additional wind ablation from loss of canopy cover likely resulting in a far greater range in snow volume losses during May 1<sup>st</sup> ( $-0.93\% \pm 11.88\%$  to  $-87.97\% \pm 7.98\%$ ). These findings are consistent with the literature which show that the presence of forests helps to retain snow in colder, continental climates where shortwave radiative inputs and wind ablation are the dominant drivers of snowmelt (Musselman et al., 2008; Lundquist et al., 2013). With postfire effects on snow albedo decay and snow albedo excluded, the postfire forest model still showed reduced peak SWE and earlier SDD than in the base model meaning that canopy loss in the study region (combined with postfire reduction in snow albedo) likely enhanced the losses in snow volume and the earlier shifts in snow retention caused by postfire effects on snow albedo alone.

### *Postfire Snow Albedo Impacts on Snow Hydrology*

Parameterizations of postfire effects on snow albedo caused reductions in peak snow volume and snow retention as long as 15 years following fire. Peak SWE within burn regions decreased across all burned forest due to parameterizations of postfire

impacts on snow albedo and snow albedo decay and, despite small increases in rates of accumulation likely due to the loss of canopy, peak SWE in the postfire albedo model was always less than that of the base model over all recovery periods with the exception of two fires (Purdy and Cliff Creek).

The combined postfire effects on forest structure and snow albedo exposed snowpack to relatively greater amounts of solar shortwave radiation that is more readily absorbed rather than reflected or refracted, increasing overall net snowpack shortwave radiation (Warren & Wiscombe, 1980). Increases in snow volume or snow retention were rarely observed and only at stages when the reductions in snow albedo caused by postfire effects had dissipated (i.e., 16+ years postfire). Further, when net increases in snow volume and snow retention occurred, they were smaller in magnitude relative to the losses incurred 1 to 15 years postfire. Forest structure change and albedo impacts caused by wildfire within the study region resulted in net reductions in snow volume for many years following the initial burn and even in the post-recovery (16 years postfire) period. Snowmelt timing occurred later only in the post-recovery period, with snow in prior recovery periods disappearing between 1 week and two months earlier than in the base model. The postfire albedo model shifted landcover within burned forests from sparsely forested to open meadows over 15 years. The reductions in snow retention in postfire forests are consistent with the literature which show that postfire effects on snow albedo result in decreased snow retention in burned forests relative to their unburned forested counterparts (Gleason et al., 2019; Smoot & Gleason, 2021; Gersh et al., 2022).

Similarly, postfire effects on snow albedo result in reductions in peak SWE and the advancing of snowmelt timing for many years following fire (Gleason et al., 2019;

Smoot & Gleason, 2021). Snowmelt timing plays an important role in annual water supply, specifically the length of the growing season and the likelihood of spring and summertime water stress and future wildfire (Harpold, 2016; Westerling, 2016; Hallema et al., 2018). A study by Harpold (2016) showed that a 1 day earlier shift in snow disappearance date can result in 1 additional day of water stress in the year (Harpold, 2016). The results here show that postfire effects on snow and forest structure can result in significant advances in SDD of between 58 and 2 days (Table 3) which, if accurate, may have implications for the increasing water stress in the 15 years beyond ignition.

However, the shifts in SDD found here are greater in magnitude than those found in the literature. Research by Smoot and Gleason found that snow in burned SNOTEL sites in the Middle Rockies disappeared between 14 to 7 days earlier 5 to 10 years postfire, less than the differences in snow disappearance between the base model and postfire albedo model (17 to 50 days earlier 5 to 10 years postfire) (Table 3) (Smoot & Gleason, 2021). The postfire shifts in SDD I found did fall in line with the 5-10 years postfire SDD shifts observed at SNOTEL sites within the Cascades region (-14 to -64 days) (Smoot & Gleason, 2021), the same region in which the postfire effects on snow albedo parameterization was developed (Gleason & Nolin, 2016). This may indicate that the postfire effect on snow albedo parameterization used in the postfire albedo model may have reflected postfire effects on snow more consistent with those found in the warmer, maritime climate of the Western Cascades. However, the results of the Smoot and Gleason (2021) study were drawn only from SNOTEL sites which are situated in open clearings within forests and at specific elevation bands. Conversely, I modeled postfire effects on snow within regions that were largely forested and across a broad

range of elevations (2168 m to 2740 m; Table 3), regions which may exhibit more variable postfire effects on snow than what can be observed from SNOTEL data alone.

*Variability in Postfire Effects on Snow Volume over Season and Recovery*

Despite identical parameterizations for albedo impacts and forest structure change being applied to each burn, the fires modeled showed varying responses in snow hydrology depending on the elevation in which they occurred. Postfire reductions in snow volume were more pronounced in snowpack at lower elevation relative snowpack at higher elevations across all burns, indicating that postfire effects on snow are more pronounced in burn regions at lower elevation. Burned forests at low elevation tended to show decreased proportional gains in March 1<sup>st</sup> SWE and increased proportional losses in April 1<sup>st</sup> and May 1<sup>st</sup> SWE relative to higher elevation burned forests. Greater losses in peak SWE at lower elevation burns meant that SDD shifts were correspondingly greater immediately following fire. Fires occurring at higher elevation exhibited increased proportional gains in SWE during the start of ablation and as early as period 1 of recovery, in the case of the Purdy burn (Figure 11). In general, postfire effects in burned forests at higher elevation caused decreased losses in peak SWE relative to burned forests at lower elevations. Conversely, burned forests at low elevations had more pronounced postfire effects on peak snow volume. Temperatures and snowpack at lower elevations are warmer and lower elevation snowpack contains lower cold content relative to snowpack at higher elevation. Postfire effects on snow albedo and forest structure increase shortwave radiative forcing on snowpack. It is likely that, in snowpack at low elevation, postfire effects on snow are more likely to shift the snowpack energy balance

negative, explaining why postfire effects on snow were more pronounced in lower elevation snowpack.

Over the recovery period, postfire effects caused losses in snow volume through every stage of recovery except in the two highest elevation burns (Purdy and Lava Mountain). The magnitude of losses in peak SWE and corresponding snow volume did not always follow a consistent trend with some burns showing the greatest losses 4-9 years postfire, indicating that the greatest postfire reductions in peak SWE and snow volume may not occur in the winter immediately following fire, but instead many years later during postfire recovery.

In contrast, SDD recovered at a steady rate throughout the recovery period, with snow disappearing earlier and earlier with each successive recovery period. Shifts in SDD were substantial and long-lasting, with snow disappearing 1-2 months earlier immediately following ignition and as much as 3 to 16 days earlier even 12 to 15 years following fire. Only once the albedo reductions due to forest fire had dissipated entirely (16+ years postfire) were any increases in snow retention observed and only in one burn region (Boulder). Shifts in SDD can result in impacts on water supply in the drier months of late spring and summer wildfire (Harpold, 2016; Westerling, 2016; Hallema et al., 2018). The disappearance of snow earlier in the year can result in drier forests in the surrounding area during late spring and summer and increase the likelihood and severity of future wildfire (Harpold, 2016; Westerling, 2016; Hallema et al., 2018).

Although postfire effects on snow albedo in the postfire albedo model had diminished or disappeared 15 years postfire, burned forests became unburned open meadows after 15 years and had not fully recovered back to a forested, pre-fire state. The

shift from forest to open meadow and the associated loss of canopy continued to cause reductions in snow volume even after the postfire effects on snow albedo had dissipated. To quantify the complete impacts of a wildfire on long-term snow evolution, future modeling using this postfire albedo parameterization in combination with models of long-term forest recovery should be incorporated into a longer-spanning modeling period.

#### *Total Effects of Postfire Impacts on Snow*

Cumulative losses in snow volume over the entire recovery period were far greater than the losses occurring immediately following fire. Losses considered over the course of the entire postfire recovery period were 7-18 times greater than the losses immediately following fire in the burns modeled for the entire recovery period (Boulder and Green Knoll fires). Further, the total losses caused by burns were related to the size of the initial event and these two fires were relatively small compared to the burns occurring late in the modeling period. The two most recent fires modeled, Cliff Creek (146 km<sup>2</sup>; Figure 8) and Roosevelt (244 km<sup>2</sup>; Figure 5) were 9 and 16 times larger than the Boulder and Green Knoll (both 15 km<sup>2</sup>). The greater extent of these later fires and significant losses of 7-10M m<sup>3</sup> of peak SWE occurring immediately postfire Cliff Creek: -8.82%/ p < 0.001; Roosevelt: -8.68%/p < 0.01) indicate that total volumetric losses over the full recovery of these burns may be on the order of hundreds of millions of volumetric peak SWE loss (Table 3). Further modeling as more data becomes available will be necessary to confirm these predictions, but such losses carry important implications for long-term water supply under a warmer, drier climate at the watershed scale.

Postfire effects from the Boulder, Bull and Cliff Creek fires caused consistent annual reductions in snow volume within the Lower Granite Creek subbasin over the 20-

year modeling period. The three fires burned over 40% of the watershed causing ablation season reductions in snow volume of  $1.14\% \pm 21.2\%$  to  $14.58\% \pm 76.1\%$  annually, an average annual reduction  $6.30\% \pm 6.95\%$ , and, in total, amounting to a 5.85% reduction in total snow volume over 20 years (Figure 12). Additional snowmelt caused by the postfire effects of these fires caused average annual increases in snowmelt of  $5.9\text{M m}^3 \pm 6.5\text{M m}^3$  per year and, over 20 years, resulted in a total of  $>94\text{M m}^3$  of added early snowmelt than would occur in no-burn conditions. As a frame of reference, the USGS stream gauge at the outlet of the Lower Granite Creek subbasin (USGS 13019438) measured an annual average streamflow volume of  $29\text{M m}^3$  per year between 1982 and 1993 (USGS, 2016). Further research would be required to determine how much of this added, early snowmelt would translate to runoff. Still, such additions have the capacity to alter resulting annual streamflow runoff and show that wildfires occurring in the seasonal snow zone have important implications for water supply and water management over long temporal scales.

### *Model Validation*

Validation of the modeled results using in-situ SWE measurements collected from within the burns showed that our modeling and parameterizations overestimated SWE in both the base model ( $+40.22 \pm 38.88\%$ ) and postfire albedo model ( $+41.61 \pm 46.29\%$ ). SWE was overestimated in both the base model and postfire albedo model and both were relatively close in accuracy ( $<1.5\%$  difference). Both the base model and postfire albedo model also overestimated SWE in the individual fires and, again, showed similar levels of accuracy between one another (Table 5). This may indicate that the postfire albedo model is underestimating postfire effects on snow and that the associated postfire effects

on forest structure and snow albedo impact snow hydrology to a greater degree than the modeled results show. However, given these overestimations were present in both models and that both showed similar accuracy relative to the observed measurements, it is likely that the calibrated base model (from which the postfire albedo parameterizations were added to) does not accurately represent SWE in the locations and on the dates at which field data was collected. This could be due to several issues including the initial calibration of SnowModel, differences in measurement methods between the field data and SNOTEL data that was assimilated into SnowModel and calibrated upon, or spatial and/or temporal variability in SWE across the study region.

First, calibration and SWE assimilation of SnowModel was performed using SNOTEL-measured SWE data and none of the SNOTEL stations were within the burn boundaries (Figure 1), meaning that calibration or assimilation of SWE within the burn regions was not possible. Second, SNOTEL stations measure SWE using a different method than that of the field validation data. SNOTEL stations measure SWE using a large bladder filled with antifreeze which weigh the overlying snow and convert to snow-water equivalent measurements (USDA-NRCS, 2020). Conversely, the SWE validation data was measured by weighing snowpack within a federal snow sampling tube and converting the weight to snow-water equivalent. The differences in how these data were collected may have resulted in a miscalibration of SnowModel due to overestimation of SWE at the SNOTEL sites or may indicate that the field validation data underestimated SWE at the field sites or possibly both. Finally, the overestimation of modeled SWE may have been due to the low spatial and temporal coverage of the field validation data. The field validation data were collected within close proximity to one another (within each

burn), over the course of ~5 weeks in a single year. Meanwhile the modeled results span multiple decades and thousands of square kilometers. Further, the field validation data represents point measurements of SWE while the modeled results were calculated in grids of 100 m<sup>2</sup>. It is possible that the differences between the observed SWE and modeled SWE could be due to temporal and/or spatial variability across snowpack within the study region. More field data collected over a wider area across the burn regions and over a longer time period will be needed to further validate the modeled results.

#### *Limitations and Future Work*

A chief limiting factor of this study lies with the mismatch between the study region that the snow albedo decay parameterization was sourced from, and the study region investigated here. The snow albedo decay parameterizations were drawn from empirical parameterizations of snow albedo decay developed by Gleason & Nolin (2016) in the Oregon Cascades – a maritime snow climate – while my study region was in the Middle Rocky Mountains – a continental snow climate. Dominant snow metamorphic processes differ between these two climates (Domine et al., 2006; Colbeck, 1982), limiting the applicability of a snow albedo decay parameterization developed in warmer, maritime climates such as the Oregon Cascades to my relatively colder, continental study region within the Rocky Mountains. In warmer maritime climates, snowpack is typically warmer and snow metamorphism is often driven by more rapid wet snow metamorphic processes (Domine et al., 2006; Colbeck, 1982). Conversely, temperatures and snowpack in continental climates are typically colder and more often driven by slower dry snow metamorphic processes (Domine et al., 2006; Colbeck, 1982). Currently, no research exists parameterizing postfire effects on snow albedo decay in continental climates and

the research by Gleason & Nolin (2016) was the only published parameterization available for inclusion in the postfire albedo model. Nevertheless, it is possible that the parametrization used here may be overestimating the rate of snow albedo decay given the faster decay rates that tend to occur in warmer climates. A slower snow albedo decay rate would change the results of the model considerably. Snow albedo would be higher on average, reducing shortwave radiative forcing on snow, shifting the snowpack energy balance positively, and slowing snow melt overall. However, the parameterization implemented in this study is flexible and the coefficients of snow albedo decay are easy to modify. As more data becomes available characterizing and parameterizing postfire effects on snow albedo decay under colder, continental climates, it would be possible to repeat similar research with snow albedo decay parameterizations that more accurately represent the conditions within my study region.

While the snow albedo decay parameterization was drawn from research using field data collected within burn regions, the forest structure component was less supported. Previous work shows that delayed tree mortality occurs at an exponentially decaying rate following fire (Angers et al., 2011; Brown & DeByle, 1987) while the parameterizations used here are linear in nature. Further, the modeling capabilities of forest structure dynamics in SnowModel are limited. SnowModel currently only has two metrics to capture forest structure dynamics: gap fraction and snow-holding depths. Gap fraction is not spatially variable so the the only way to model varying forest structure within burn regions alone is to modify the snow-holding depth value and associated leaf area index. While the snow-holding depths do play important roles in SnowModel's physically-based calculations, more work should be done in the future to incorporate

more descriptive metrics of forest structure, specifically the three-dimensional capacity of vegetation to intercept and modify the snow-energy balance. Such parameterizations will allow more accurate modeling of postfire impacts on forest structure and the resulting impacts on snowpack in general.

Another limiting factor in this study is the small number of in-situ SWE observations available for calibration of SnowModel and the limited spatial and temporal extent of in-situ SWE validation data. The study region only contains nine SNOTEL sites and thus only nine potential points in which to base the calibration of SnowModel upon. SNOTEL sites are placed within a relatively narrow band of elevations and in a limited variety of landcover types (Meromy et al., 2012; Molotch and Bales, 2005). These limitations inhibit this study's ability to capture variability in snowpack both spatially and over elevation, which affects the accuracy of the modeled results. Validation of the modeled results was limited due to the small number of data points available for validation and the low spatial and temporal extent of those data. While the data available was highly valuable and diligently retrieved, they were collected in a short span of time and within close proximity to one another within each fire region relative the 20-year time scale and thousand square-kilometer spatial scales modeled in this study. The fires modeled in this study occurred over large extents and the postfire effects on snow and associated recovery span many years meaning that field data, while useful, is likely insufficient to validate processes modeled over such temporal and spatial scales. Future work will attempt to use remotely-sensed measurements of snow-covered area and snow albedo from the MODSCAG dataset sourced from Snow Today through the NSIDC

(Ashcroft & Wentz, 2013), allowing for a more spatially- and temporally-extensive validation of the base model, postfire forest model, and postfire albedo model.

Finally, the results of this study show that postfire effects on snow hydrology result in significant reductions in snow volume by May 1<sup>st</sup> for many years following fire and earlier snow disappearance dates for as long as 15 years following fire. While the volume and earlier snowmelt was quantified in this study, I did not perform any modeling to determine how this earlier snowmelt affects the hydrology of burned watersheds and, critically, what the fate of additional, earlier runoff is. Future research should pair results of this study with hydrological runoff models such as the Hydrologic Engineering Center Hydrologic Modeling System (USACE-HEC, 2012) or others to quantify additions to springtime runoff and associated impacts on water storage and summertime water supplies.

## CONCLUSION

Wildfire has significant effects on canopy cover and radiative forcing on snow for decades following fire and thus has the capacity to significantly alter snow evolution and, by extension, water supply over long time scales. This study assessed the long-term water supply impacts of postfire effects on the snow-mass energy balance by incorporating time-varying forest structure change and an empirical burned albedo decay function into SnowModel. The results of the parameterized (postfire forest and postfire albedo) runs were compared with those of a base model and a postfire forest model to quantify and partition the impacts of wildfire on snowpack evolution. I quantified the resulting impacts of forest structure change and albedo modification on modeled peak snow water equivalent (peak SWE), snow disappearance date (SDD), and total SWE volume reductions over a 20-year time scale and over a >7 thousand square kilometer area. Spatially-variate changes in SWE due to postfire effects were compared both over the snow season (accumulation, start of ablation, and ablation) and throughout the 15-year postfire recovery period.

Postfire degradation of canopy allowed for slightly greater accumulation rates in the modeled burns, but postfire reductions in canopy shading and postfire effects on snow albedo and snow albedo decay generally resulted in severe reductions in SWE at start of ablation and during the melt season. Volumetric SWE was reduced following fire and snow was observed to disappear up to 5 weeks earlier relative to the base model. Over the 15 years of postfire recovery, seasonal differences in SWE, volumetric SWE reductions, and SDD shifted closer to base model levels, but remained negative in nearly every burn modeled. The most significant postfire reductions in peak SWE were observed in burn

forests at lower elevation. Across the 15 year postfire recovery period, the greatest reductions in SWE and SDD due to postfire effects on snow did not occur immediately following fire, but instead 4-9 years following fire.

Following the 15 year postfire recovery period (16 years postfire), one fire showed increased volumetric SWE and later SDD relative to the base model, but another still showed reductions in both metrics 16 years following ignition. Burned forests approach snow albedo values similar to that of open regions over 15 years following burn indicating that such regions have not yet fully recovered back to a forested state by this time. Future work should use similar parameterizations over longer time scales (>20 years) to better capture and quantify postfire impacts on snow over the entire recovery to a pre-fire state.

The results of this study show that wildfire has significant and persistent impacts on snow hydrology and water supply that last decades beyond the initial burn event. Quantification of changes in snow volume and snow melt on the snow-mass energy-balance using physically-based, parameterized snow models provide information critical to our understanding of the long-term impacts of an increasingly-severe fire regime on the quantity and timing of our precious water resources.

## FIGURES AND TABLES

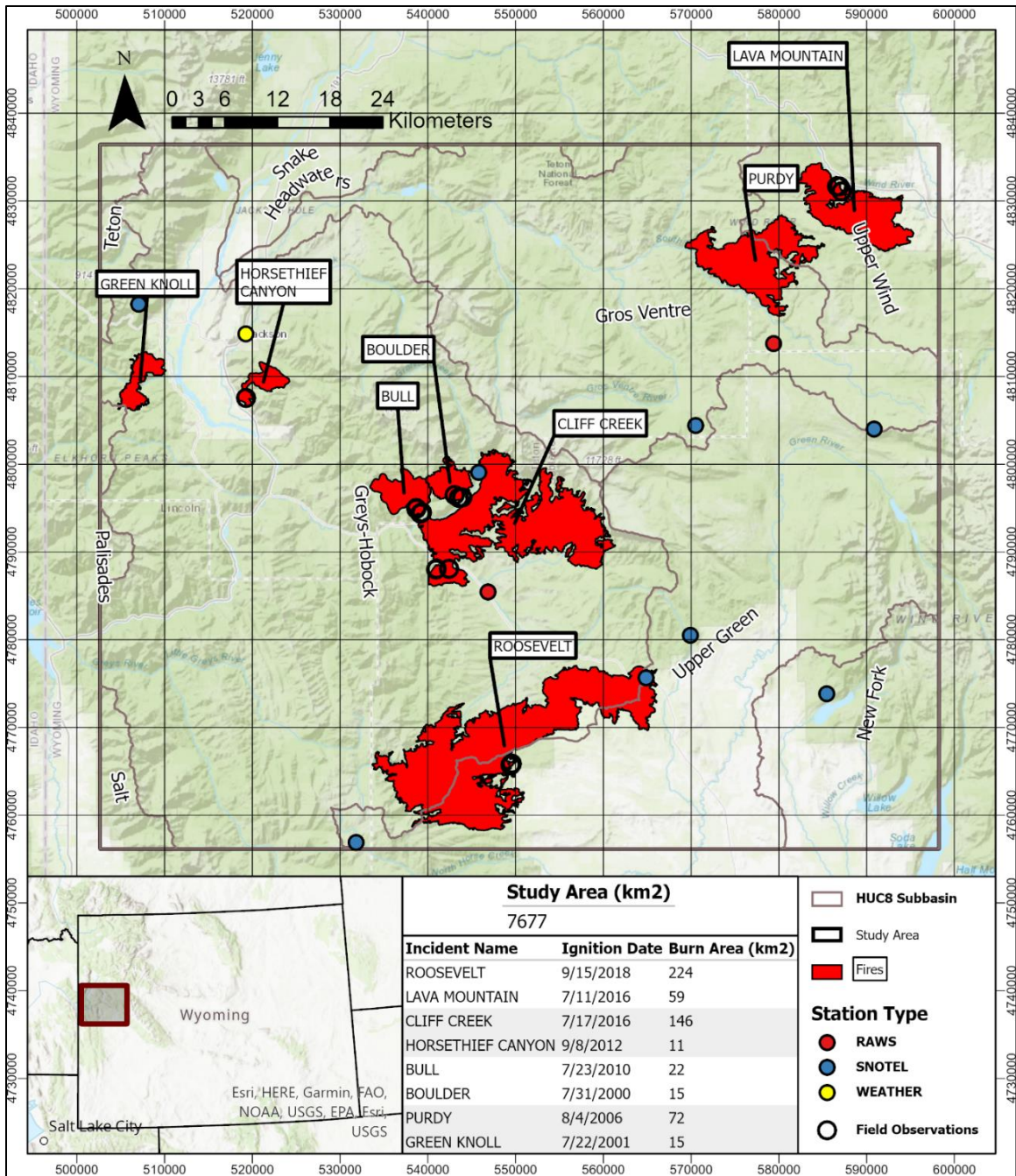


Figure 1: A map of the study region and modeling bounds. The map includes MTBS fire boundaries of the eight fires that occurred in the study region over the modeling time period along with their ignition date, incident type, and total burn area. The location and type of meteorological stations that the in-situ meteorological forcing data was drawn from are shown and the boundaries of the HUC-8 sub-basins and their names are also displayed.

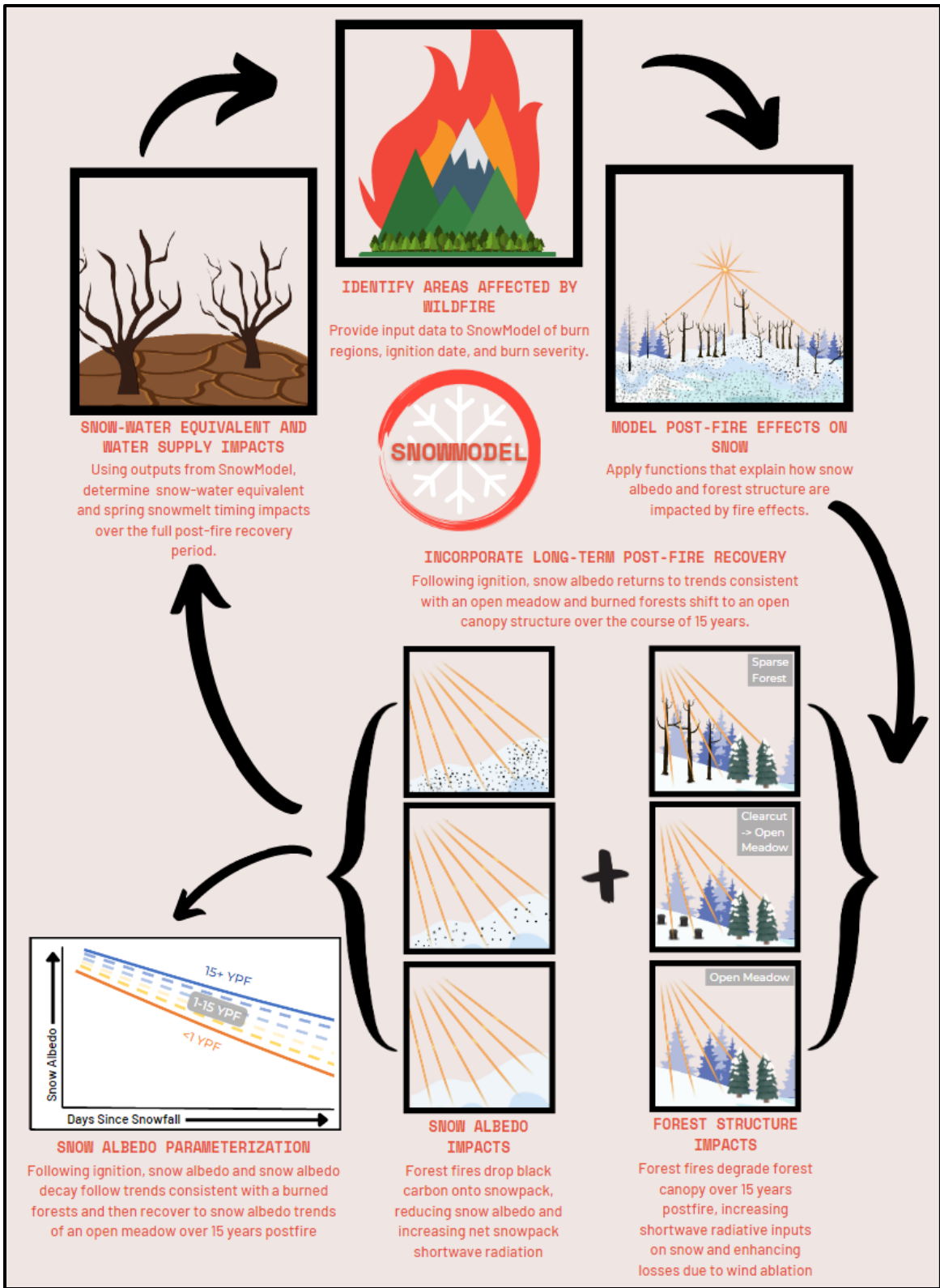


Figure 2: A conceptual model of the postfire effects on snow captured by the postfire albedo and postfire forest models and a simplified explanation of the modeling methods.

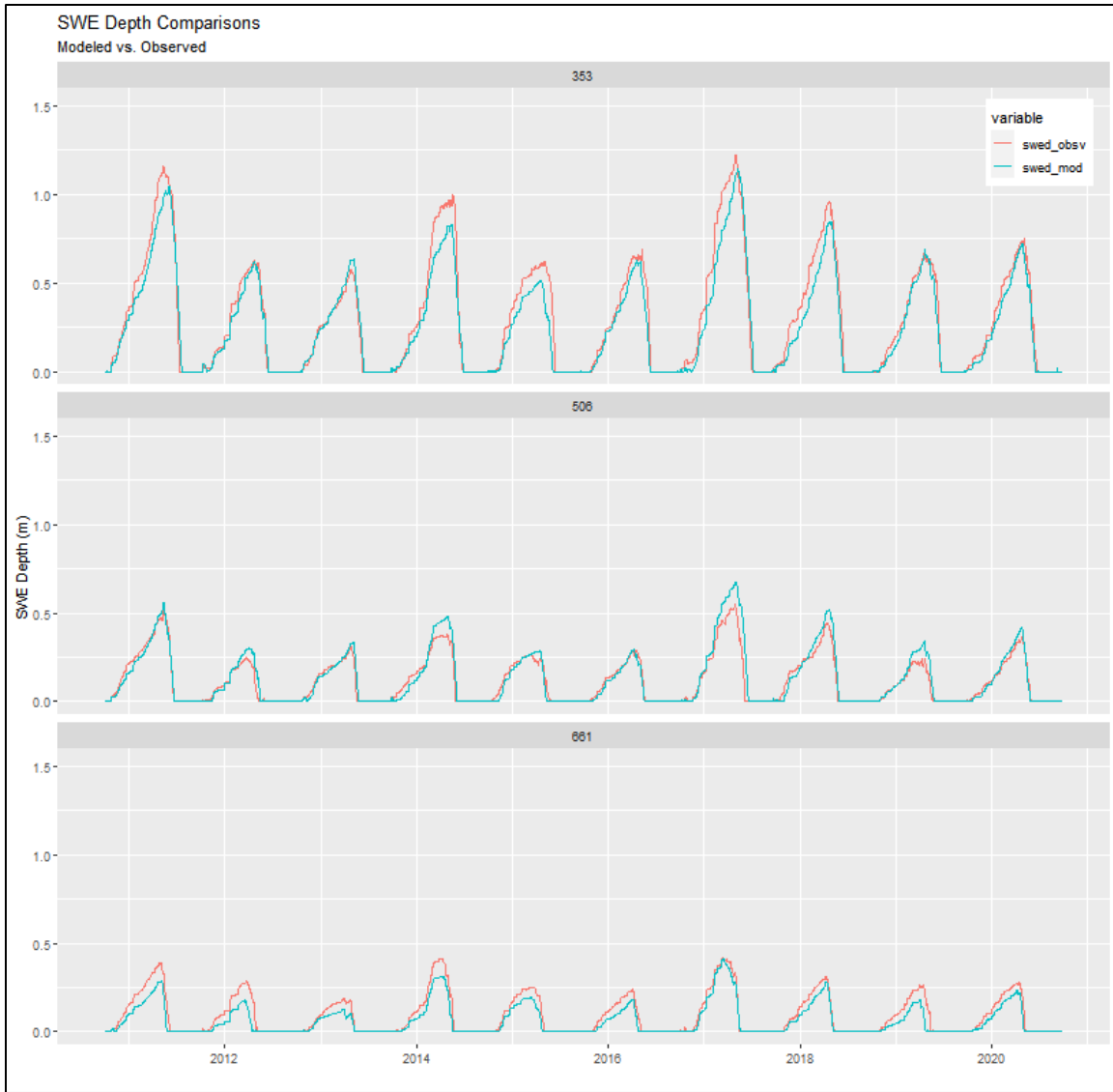


Figure 3: A subset of the calibration plots following calibration of SnowModel's SWE outputs for 10 years of the study period.

Table 1: List of meteorological stations used as the meteorological forcing data input or as validation data in SnowModel. Relevant metadata is provided including station type, data source, station ID number (\* = validation station only), elevation in meters, easting and northing coordinates (CRS: NAD83 UTM12N), and date of the start of record.

Station Name	Type	Source	Station ID	Elevation (m)	Easting (m)	Northing (m)	Start of Record
Blind Bull Sum	SNOTEL	USDA-NRCS	353*	2637	531829	4756891	10/1/1978
East Rim Divide	SNOTEL	USDA-NRCS	460*	2417	564881	4775668	10/1/1984
Granite Creek	SNOTEL	USDA-NRCS	497*	2063	545799	4799058	10/1/1987
New Fork Lake	SNOTEL	USDA-NRCS	689*	2542	507065	4818219	10/1/1984
Gros Ventre Summit	SNOTEL	USDA-NRCS	506	2667	570509	4804425	4/1/1976
Gunsight Pass	SNOTEL	USDA-NRCS	555	2993	579829	4788969	9/1/1998
Kendall R.S.	SNOTEL	USDA-NRCS	597	2359	569894	4780482	10/1/1984
Loomis Park	SNOTEL	USDA-NRCS	661	2512	585471	4773860	10/1/1979
Phillips Bench	SNOTEL	USDA-NRCS	944	2499	590870	4803994	3/1/1976
Hoback Wyoming	RAWS	DRI-WRCS	481302	2050	546858	4785438	6/1/1996
Raspberry Wyoming	RAWS	DRI-WRCS	481307	2682	579399	4813724	6/1/1985
Jackson Airport	Weather	NOAA-CDO	USC00484910	1893	519283	4814846	1/1/1893

Table 2: Table showing the final performance statistics of SnowModel following pre-parameterization calibrations. The four statistics (described in the Preliminary Results section) are shown for each of the nine SNOTEL stations within the study region and the overall performance statistics are shown on the last row. The performance thresholds used for this study are also shown for each of the four statistics.

Station Name	Station ID	Elevation (m)	Easting (m)	Northing (m)	Start of Record	RSR (<0.70)	NSE (>0.50)	R <sup>2</sup> (>0.60)	PBIAS ( x <15%)
Blind Bull Sum	353*	2637	531829	4756891	10/1/1978	0.34	0.89	0.90	5.10
East Rim Divide	460*	2417	564881	4775668	10/1/1984	1.03	-0.06	0.81	60.80
Granite Creek	497*	2063	545799	4799058	10/1/1987	0.29	0.91	0.93	-6.10
New Fork Lake	689*	2542	507065	4818219	10/1/1984	0.57	0.68	0.77	11.80
Gros Ventre Summit	506	2667	570509	4804425	4/1/1976	0.68	0.54	0.87	28.50
Gunsight Pass	555	2993	579829	4788969	9/1/1998	0.31	0.90	0.95	-14.60
Kendall R.S.	597	2359	569894	4780482	10/1/1984	0.28	0.92	0.92	2.20
Loomis Park	661	2512	585471	4773860	10/1/1979	0.34	0.89	0.93	10.20
Phillips Bench	944	2499	590870	4803994	3/1/1976	0.49	0.76	0.90	23.10
Overall						0.44	0.81	0.85	11.40

**Table 3: Calculations of the differences in volumetric SWE (<1 year postfire, total, and per period) and differences in snow disappearance date (SDD) between the base model and burn-recovery parameterized model. Cells are colored in severity of the change for each burn, with red indicating more severe losses and blue indicating relative gains. The ignition year, total burn area, average elevation, and altitudinal variability for each burn region are included above. Asterisks are also shown on all SWE metrics denoting the level of significant difference between the base model and postfire albedo model (blank: not significantly different, \*:  $p < 0.05$ , \*\*:  $0.001 < p < 0.01$ ; \*\*\*:  $p < 0.001$ ).**

	BOULDER				GREEN KNOLL				PURDY				BULL			
<b>Burn Information</b>																
Ignition Year	2000				2001				2006				2010			
Burn Area	15 km <sup>2</sup>				15 km <sup>2</sup>				72 km <sup>2</sup>				22 km <sup>2</sup>			
Elevation (Mean)	2291 m				2168 m				2740 m				2323 m			
Elevation (Standard Dev)	119 m				144 m				143 m				176 m			
<b>Total Peak SWE Change</b>																
Immediate Peak SWE Loss (<1 YPF)	** -763,846 m <sup>3</sup> -8.98%				* -484,672 m <sup>3</sup> -2.81%				** -8,626,975 m <sup>3</sup> -13.43%				-1,118,566 m <sup>3</sup> -12.17%			
Total Peak SWE Loss (1-15 YPF)	*** -5,531,741 m <sup>3</sup> -3.83%				*** -8,858,005 m <sup>3</sup> -7.51%				-16,226,986 m <sup>3</sup> -8.35%				* -19,031,592 m <sup>3</sup> -10.99%			
<b>Total Peak SWE Change Averaged Over Period</b>																
	SD				SD				SD				SD			
Period 1	*** -804,661 m <sup>3</sup>	454,497 m <sup>3</sup>	-10.08%	5.02%	*** -474,269 m <sup>3</sup>	33,227 m <sup>3</sup>	-7.26%	0.40%	** -2,926,595 m <sup>3</sup>	3,017,555 m <sup>3</sup>	-5.63%	6.49%	*** -2,990,987 m <sup>3</sup>	1,769,086 m <sup>3</sup>	-19.32%	13.96%
Period 2	** -718,475 m <sup>3</sup>	473,466 m <sup>3</sup>	-8.17%	6.89%	** -1,889,429 m <sup>3</sup>	621,289 m <sup>3</sup>	-26.02%	10.17%	-4,735,668 m <sup>3</sup>	412,196 m <sup>3</sup>	-8.89%	1.09%	*** -1,504,158 m <sup>3</sup>	252,548 m <sup>3</sup>	-10.38%	2.02%
Period 3	-1,083,367 m <sup>3</sup>	342,718 m <sup>3</sup>	-11.81%	3.12%	** -873,168 m <sup>3</sup>	435,253 m <sup>3</sup>	-10.58%	8.25%	*** -1,459,509 m <sup>3</sup>	537,322 m <sup>3</sup>	-3.09%	1.43%	-2,048,956 m <sup>3</sup>	2,037,051 m <sup>3</sup>	-10.74%	7.70%
Period 4	*** -493,460 m <sup>3</sup>	120,266 m <sup>3</sup>	-4.68%	1.27%	-725,179 m <sup>3</sup>	216,023 m <sup>3</sup>	-10.32%	5.22%	*** -639,712 m <sup>3</sup>	402,375 m <sup>3</sup>	-1.06%	1.49%	-106,573 m <sup>3</sup>	---	-0.64%	---
Period 5	*** -505,844 m <sup>3</sup>	248,177 m <sup>3</sup>	-5.35%	2.97%	** -900,215 m <sup>3</sup>	682,678 m <sup>3</sup>	-12.20%	11.17%	** -1,018,039 m <sup>3</sup>	1,142,487 m <sup>3</sup>	2.25%	1.96%	---	---	---	---
Post-Rec.	*** 196,334 m <sup>3</sup>	---	2.32%	---	*** -241,246 m <sup>3</sup>	---	-2.20%	---	---	---	---	---	---	---	---	---
<b>SDD Shift Averaged Over Period</b>																
	SD				SD				SD				SD			
Period 1	-58 days	9 days	---	---	-37 days	3 days	---	---	-55 days	7 days	---	---	-42 days	7 days	---	---
Period 2	-38 days	11 days	---	---	-27 days	4 days	---	---	-44 days	5 days	---	---	-50 days	11 days	---	---
Period 3	-30 days	2 days	---	---	-34 days	8 days	---	---	-40 days	9 days	---	---	-46 days	6 days	---	---
Period 4	-31 days	2 days	---	---	-17 days	3 days	---	---	-21 days	2 days	---	---	-33 days	---	---	---
Period 5	-16 days	3 days	---	---	-3 days	5 days	---	---	-11 days	2 days	---	---	---	---	---	---
Post-Rec.	-2 days	---	---	---	6 days	---	---	---	---	---	---	---	---	---	---	---
<b>Burn Information</b>																
Ignition Year	2012				2016				2016				2018			
Burn Area	11 km <sup>2</sup>				59 km <sup>2</sup>				146 km <sup>2</sup>				224 km <sup>2</sup>			
Elevation (Mean)	2281 m				2565 m				2321 m				2419 m			
Elevation (Standard Dev)	142 m				125 m				181 m				177 m			
<b>Total Peak SWE Change</b>																
Immediate Peak SWE Loss (<1 YPF)	*** -1,871,501 m <sup>3</sup> -31.91%				*** -7,821,564 m <sup>3</sup> -17.05%				*** -7,885,836 m <sup>3</sup> -8.82%				** -10,601,780 m <sup>3</sup> -8.68%			
Total Peak SWE Loss (1-15 YPF)	** -7,727,252 m <sup>3</sup> -12.45%				** -8,552,127 m <sup>3</sup> -5.96%				** -11,490,365 m <sup>3</sup> -0.76%				** -20,493,335 m <sup>3</sup> -8.16%			
<b>Total Peak SWE Change Averaged Over Period</b>																
	SD				SD				SD				SD			
Period 1	*** -1,306,536 m <sup>3</sup>	842,744 m <sup>3</sup>	-19.80%	15.17%	*** -5,652,149 m <sup>3</sup>	757,521 m <sup>3</sup>	-15.18%	1.65%	*** -12,755,335 m <sup>3</sup>	4,018,615 m <sup>3</sup>	-12.74%	4.46%	** -12,476,524 m <sup>3</sup>	3,473,264 m <sup>3</sup>	-10.03%	3.29%
Period 2	** -1,278,416 m <sup>3</sup>	342,543 m <sup>3</sup>	-16.33%	4.39%	** 1,680,523 m <sup>3</sup>	---	5.66%	---	*** -6,707,108 m <sup>3</sup>	---	-7.81%	---	---	---	---	---
Period 3	-983,761 m <sup>3</sup>	170,097 m <sup>3</sup>	-12.45%	2.12%	---	---	---	---	---	---	---	---	---	---	---	---
Period 4	---	---	---	---	---	---	---	---	---	---	---	---	---	---	---	---
Period 5	---	---	---	---	---	---	---	---	---	---	---	---	---	---	---	---
Post-Rec.	---	---	---	---	---	---	---	---	---	---	---	---	---	---	---	---
<b>SDD Shift Averaged Over Period</b>																
	SD				SD				SD				SD			
Period 1	-44 days	9 days	---	---	-33 days	3 days	---	---	-37 days	1 days	---	---	-38 days	4 days	---	---
Period 2	-42 days	9 days	---	---	-22 days	---	---	---	-33 days	---	---	---	---	---	---	---
Period 3	-28 days	7 days	---	---	---	---	---	---	---	---	---	---	---	---	---	---
Period 4	---	---	---	---	---	---	---	---	---	---	---	---	---	---	---	---
Period 5	---	---	---	---	---	---	---	---	---	---	---	---	---	---	---	---
Post-Rec.	---	---	---	---	---	---	---	---	---	---	---	---	---	---	---	---

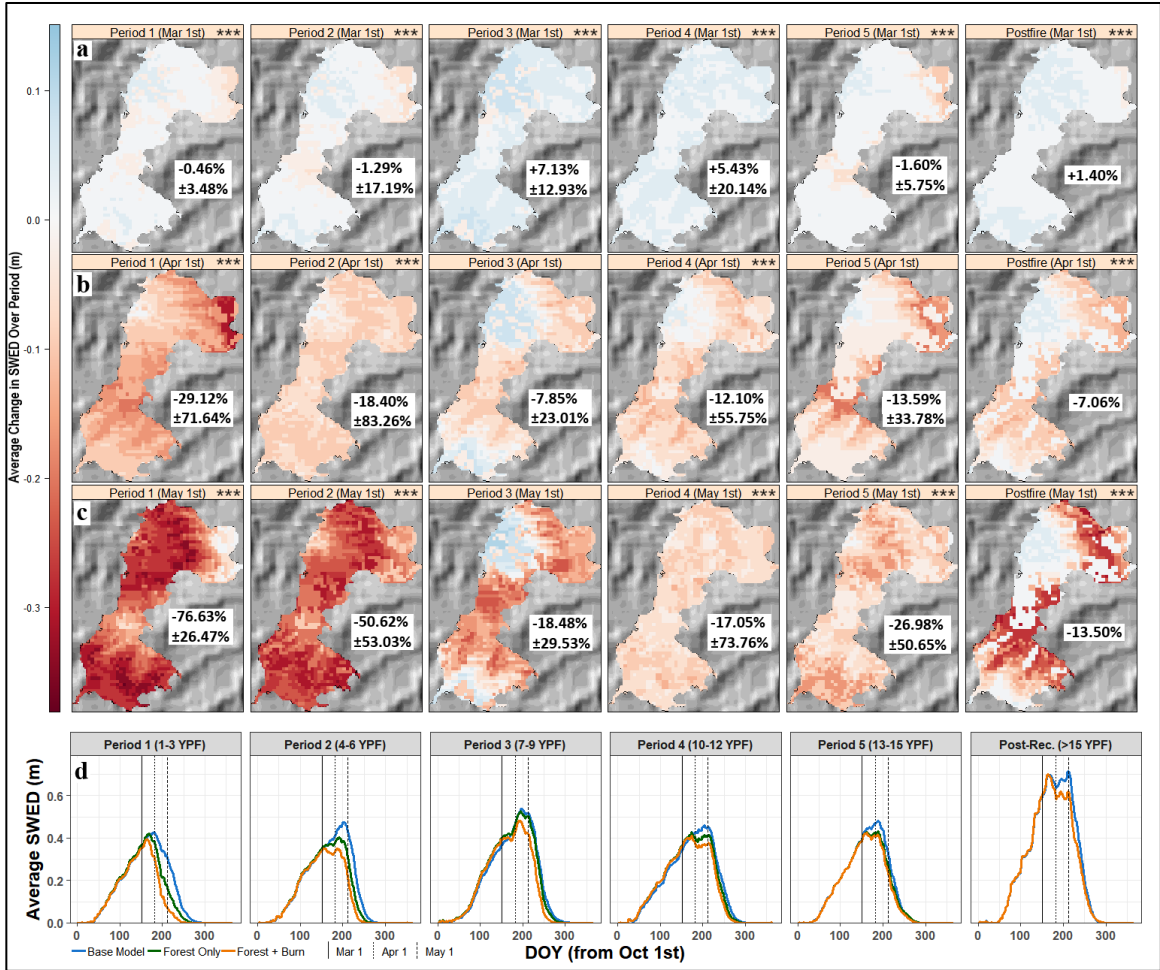


Figure 4: Matrix of rasters of the Green Knoll fire (Ignition Year: 2001) showing the change in snow-water equivalent depth (SWED) between the base model and parameterized model. Each row of rasters is labeled (a to c) for reference. A differenced raster is shown for accumulation (a; March 1<sup>st</sup>), start of ablation (b; April 1<sup>st</sup>), and ablation (c; May 1<sup>st</sup>) and each raster represents a three-year average over each successive recovery period following fire (e.g. Period 1 = 1-3 years postfire, Period 2 = 4-6 years postfire, etc.). Within each raster, the average proportional difference in SWE between the postfire effect and recovery model and the base model. Next to the title of each raster, results of significance testing between the base and postfire albedo model are displayed (blank: not significantly different, \*:  $p < 0.05$ , \*\*:  $0.001 < p < 0.01$ ; \*\*\*:  $p < 0.001$ ). Beneath the rasters are niva plots (row d) showing the average snow-water equivalent depth within the burn region over the water year, once again averaged over each 3-year period following fire. The results of the base model, forest only model, and fully-parameterized model are displayed along with lines showing the position of the accumulation/start of ablation/ablation dates.

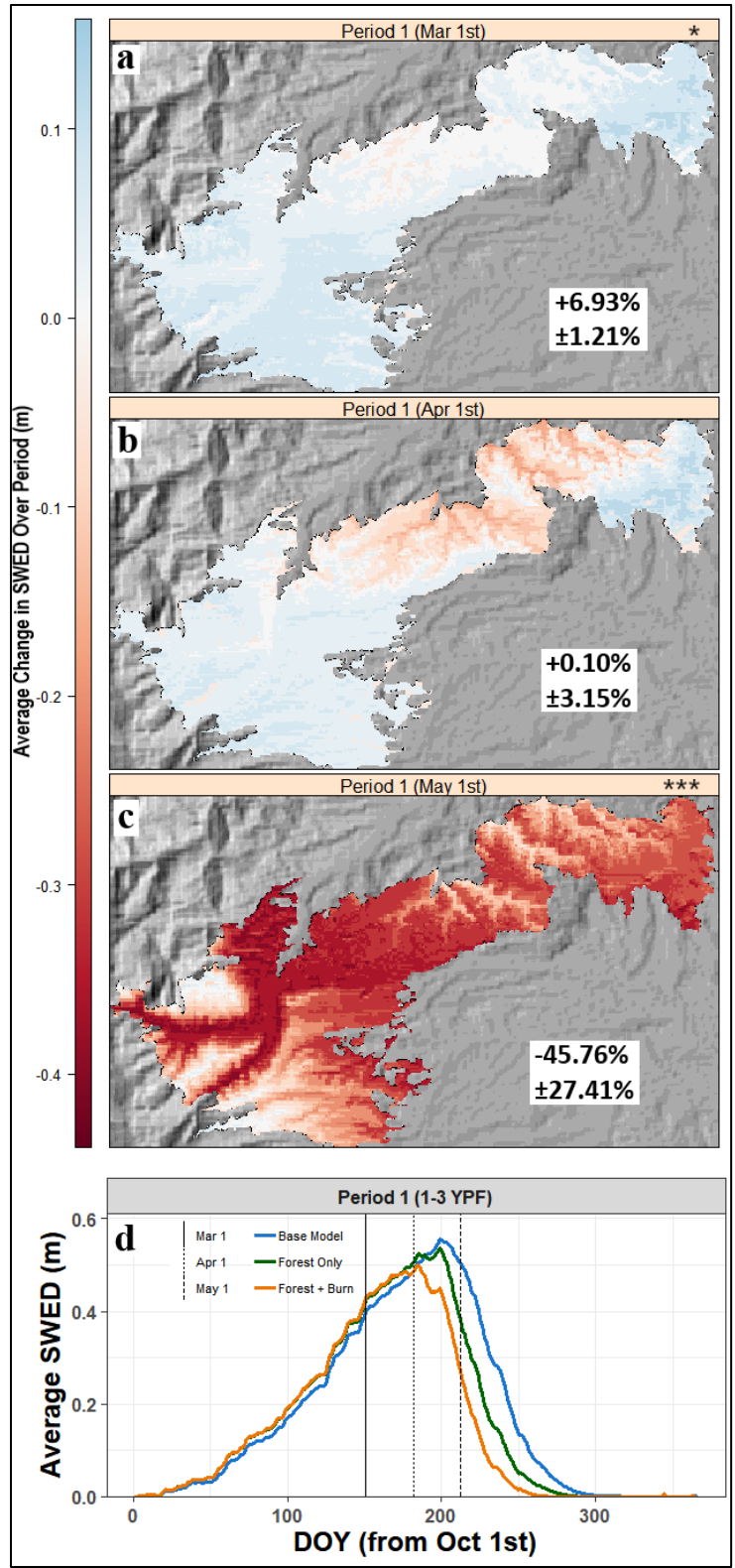


Figure 5: A combined raster/nivea matrix similar to Figure 7 for the Roosevelt fire (Ignition Year: 2018).

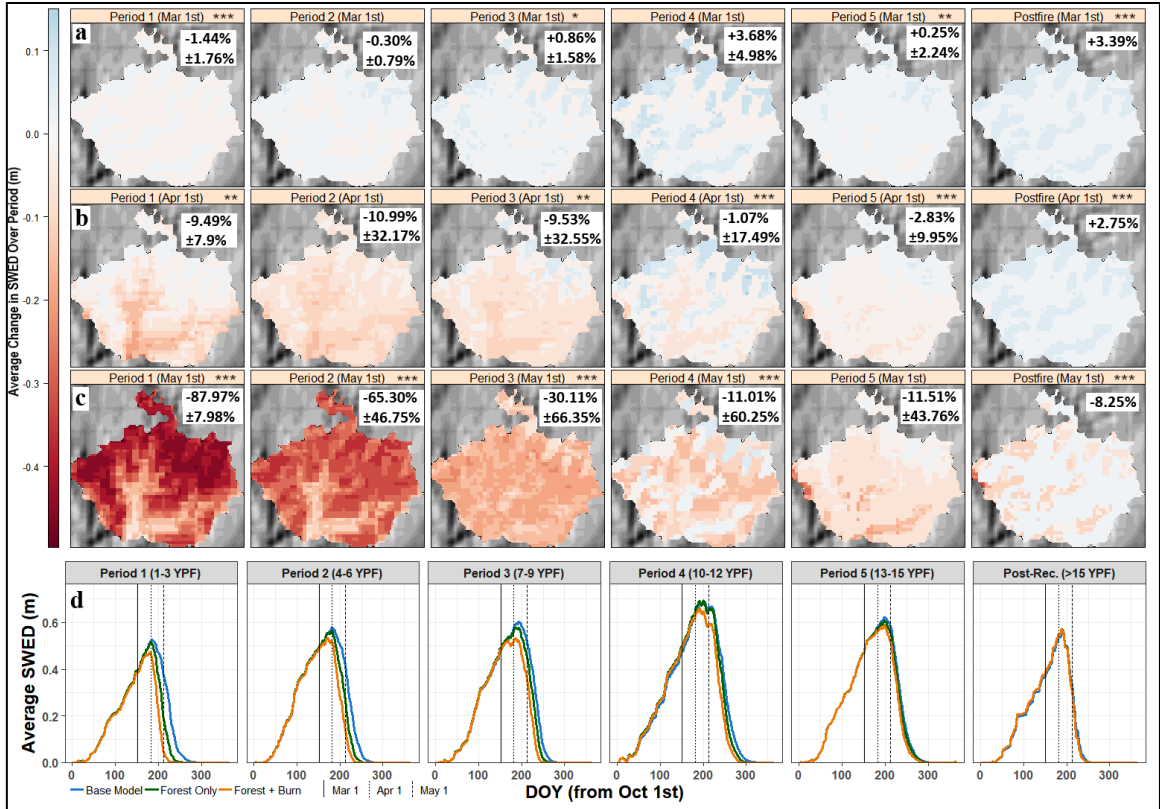


Figure 6: A combined raster/nivea matrix similar to Figure 7 for the Boulder fire (Ignition Year: 2000).

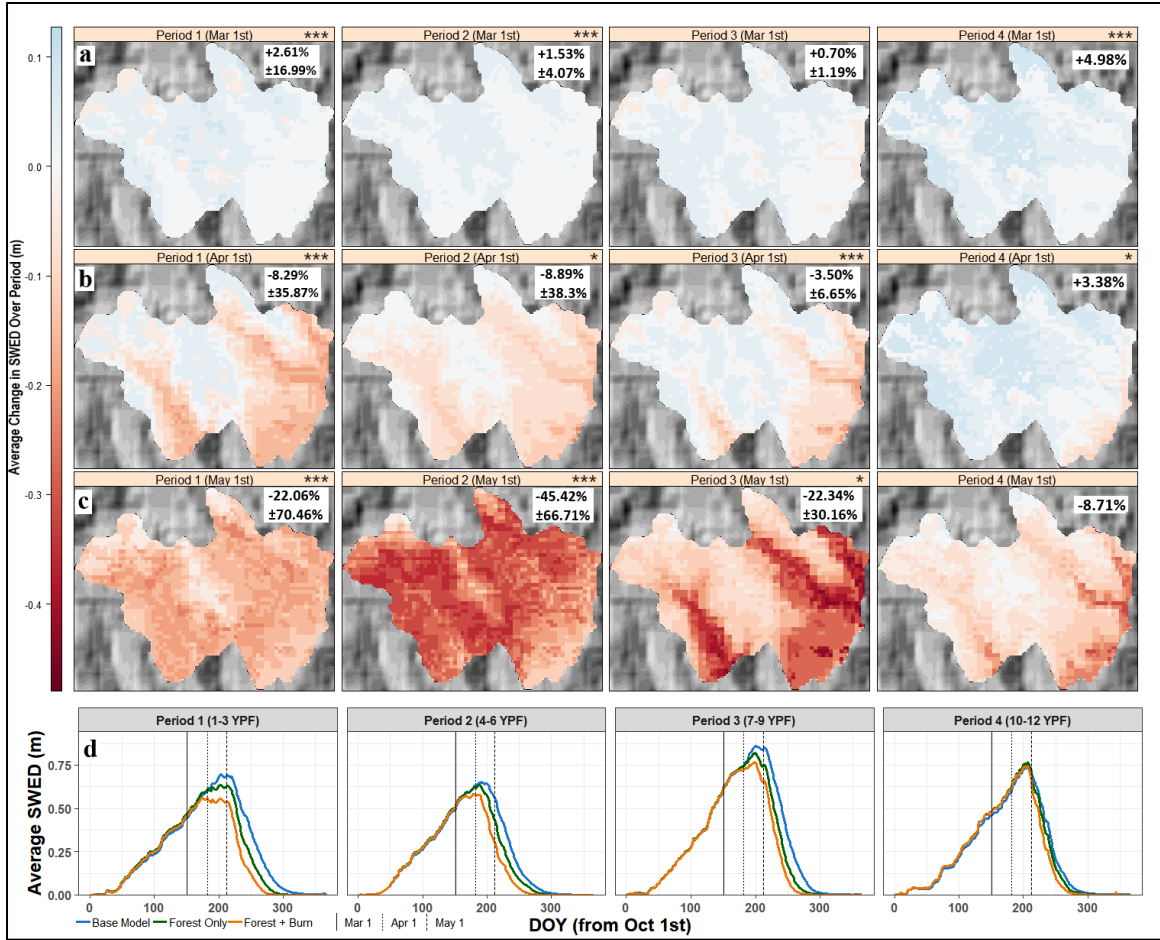


Figure 7: A combined raster/nivea matrix similar to Figure 7 for the Bull fire (Ignition Year: 2010).

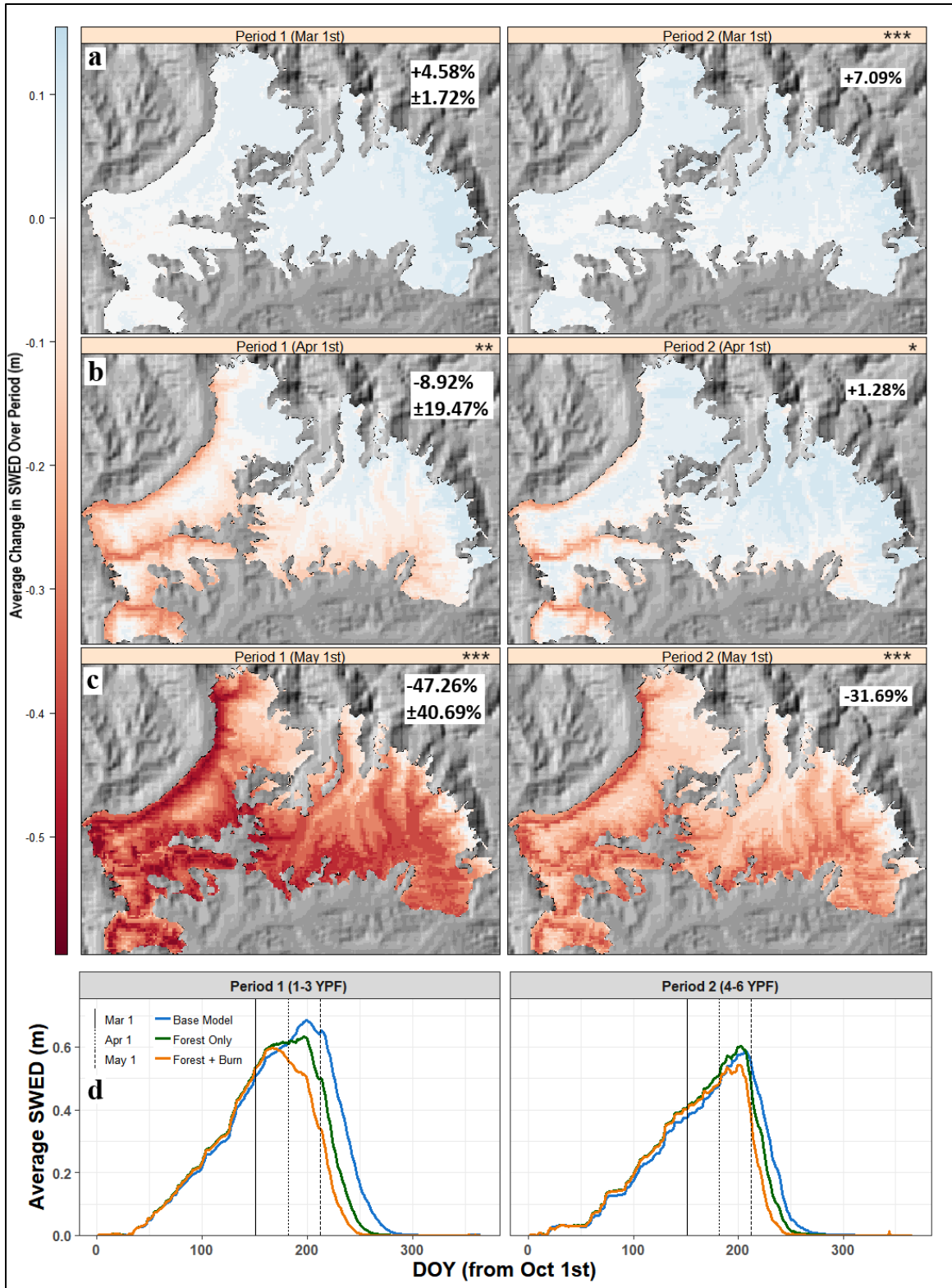


Figure 8: A combined raster/nivea matrix similar to Figure 7 for the Cliff Creek fire (Ignition Year: 2016).

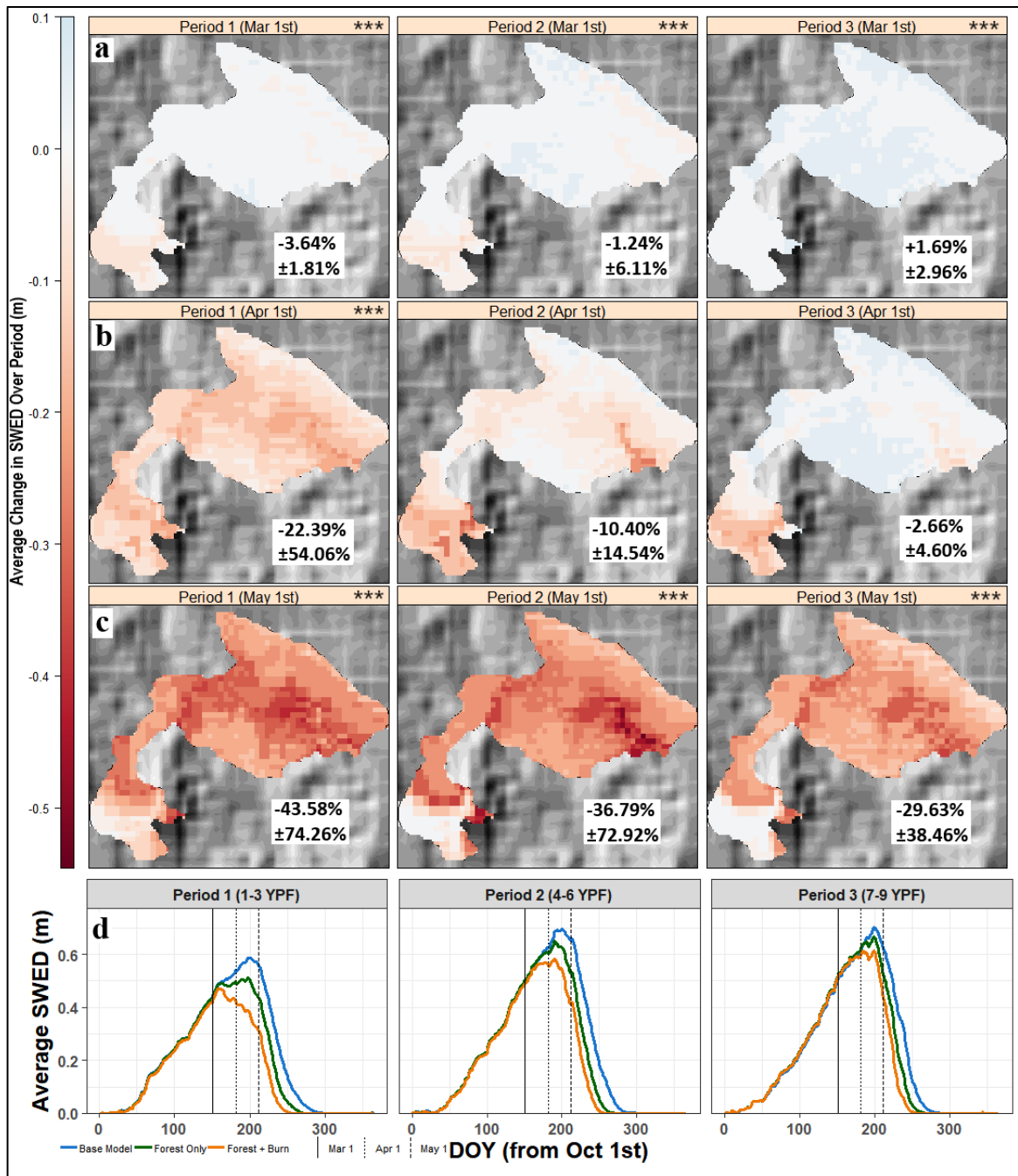


Figure 9: A combined raster/nivea matrix similar to Figure 7 for the Horsethief Canyon fire (Ignition Year: 2012).

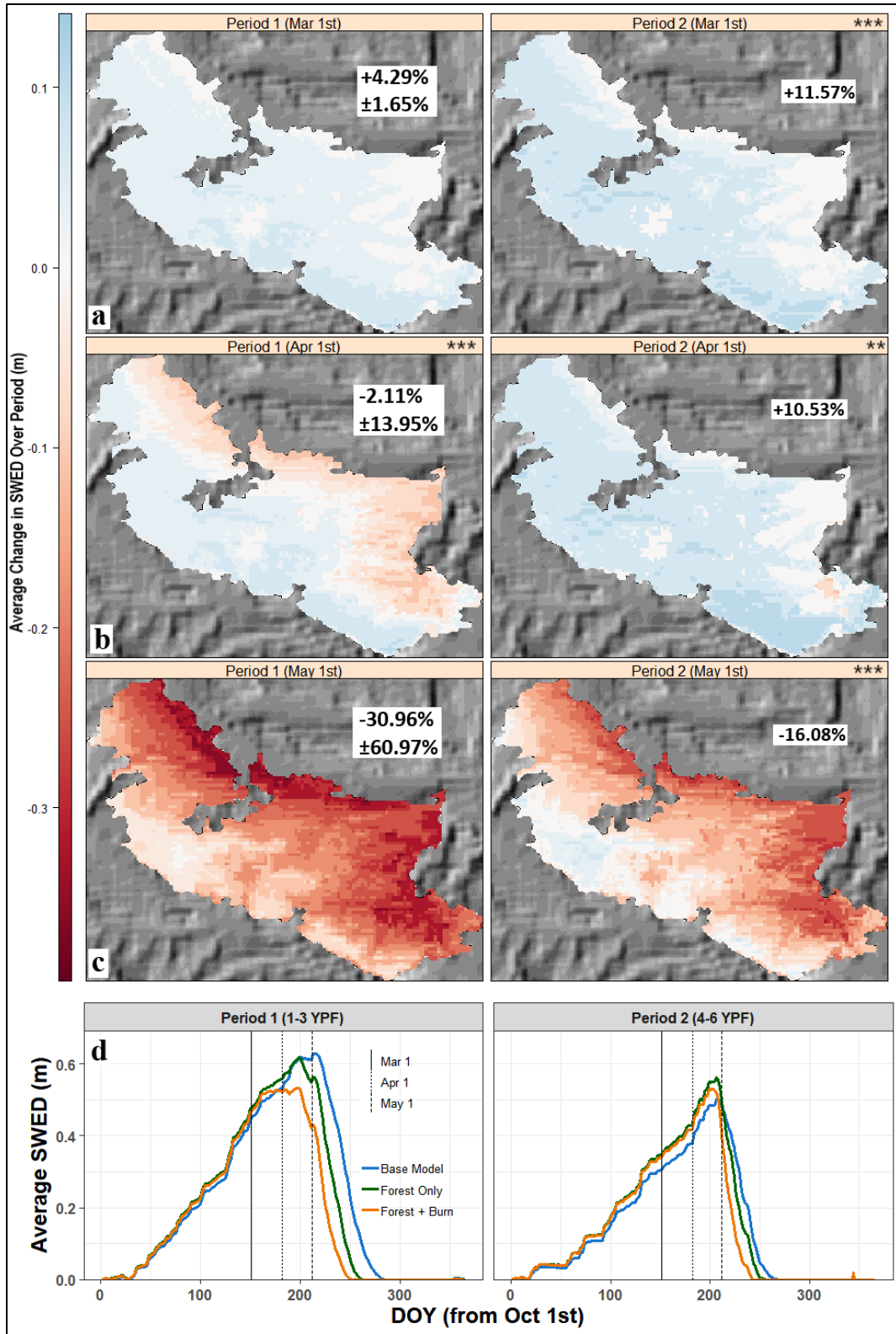


Figure 10: A combined raster/nivea matrix similar to Figure 7 for the Lava Mountain fire (Ignition Year: 2016).

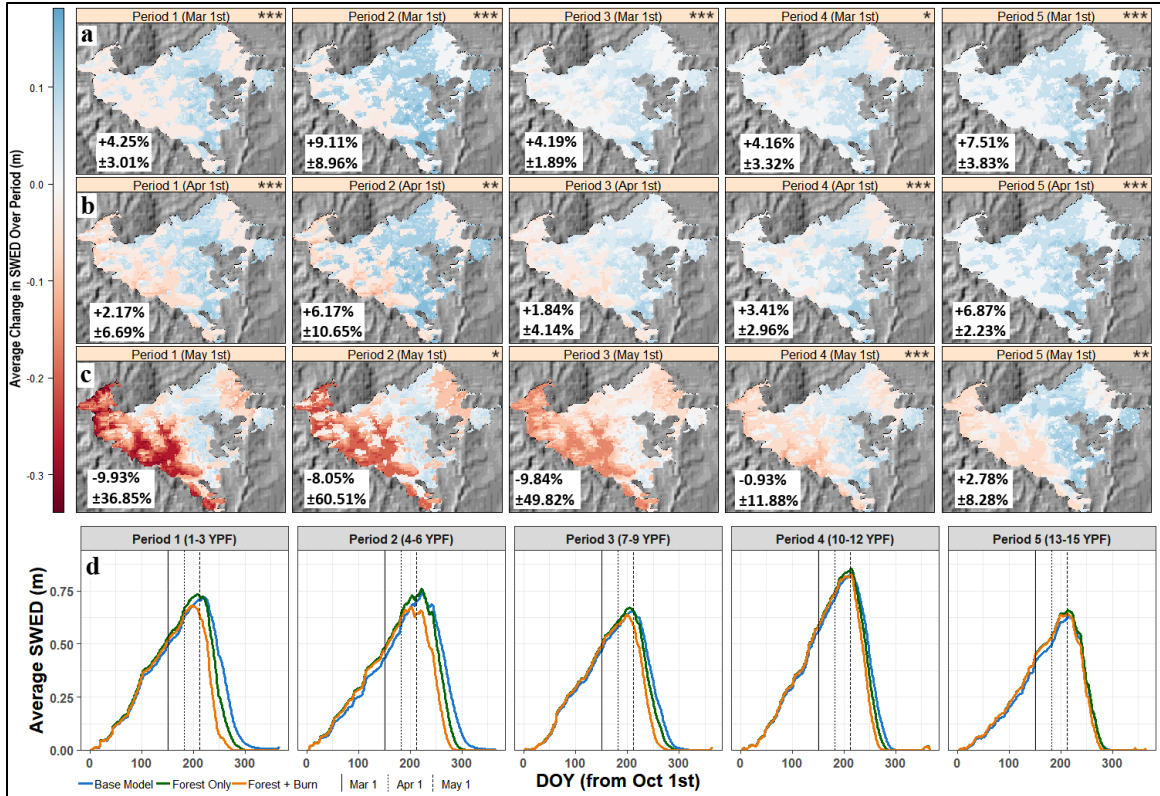


Figure 11: A combined raster/nivea matrix similar to Figure 7 for the Purdy fire (Ignition Year: 2006).

Table 4: Average annual proportional peak SWE loss between the postfire effect and recovery model and the baseline model. Fires are ordered by increasing elevation to highlight the trend in decreasing average proportional peak SWE losses over increasing elevation. Elevation and losses are colored to indicate the magnitude relative to the range in the given value.

Fire	Green Knoll	Horsethief Canyon	Boulder	Cliff Creek	Bull	Roosevelt	Lava Mountain	Purdy
Ignition Year	2001	2012	2000	2016	2010	2018	2016	2006
Elevation (mean)	2168	2281	2291	2321	2323	2419	2565	2740
Elevation (Std. Dev.)	144	142	119	181	176	177	125	143
Avg. Annual Peak SWE Loss	-7.20%	-6.69%	-2.17%	-4.07%	-4.16%	-4.26%	-3.08%	-0.54%

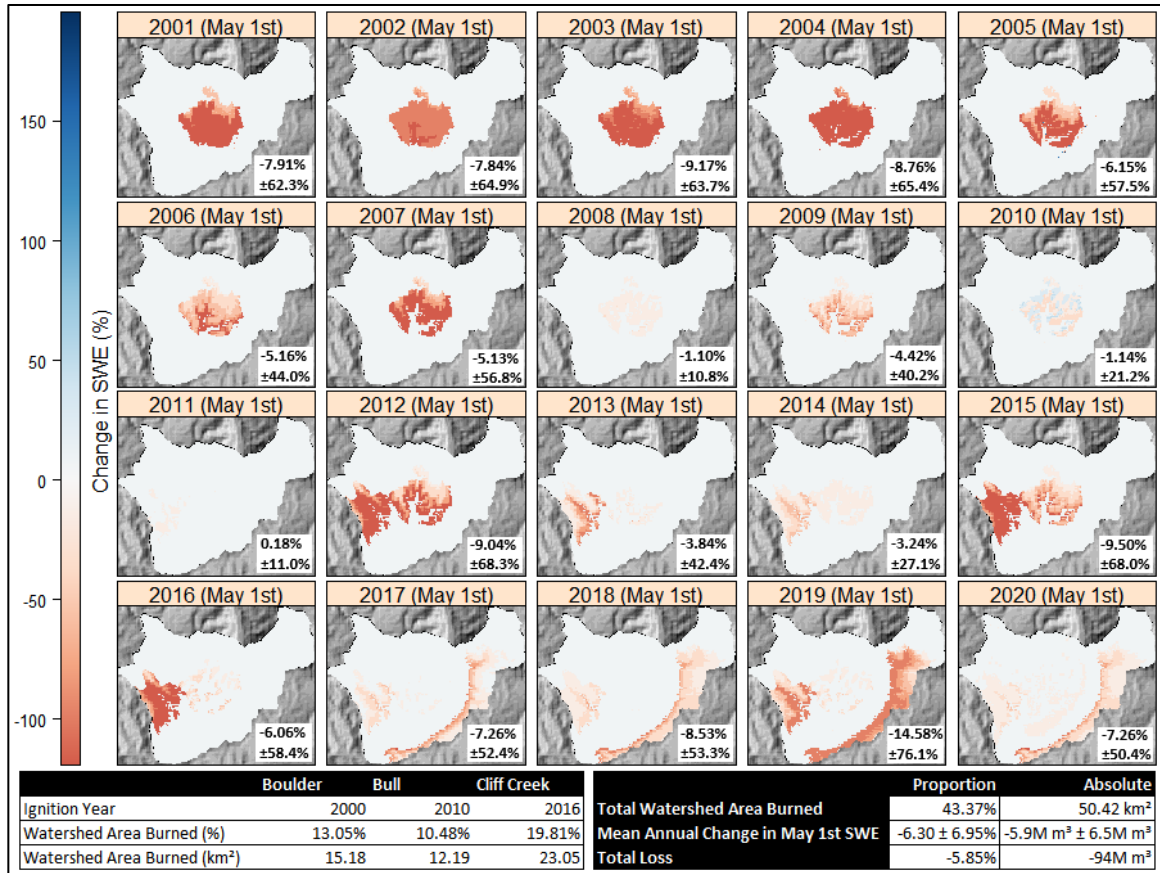


Figure 12: Spatial analysis of watershed scale impacts of postfire effects and recovery in the Lower Granite Creek subbasin (HUC12) during the ablation period (May 1<sup>st</sup>) for every modeled year. Reductions in SWE due to postfire effects are presented as proportional differences between the postfire effect on snow albedo and forest structure model and the base model. SWE data is shown only for areas within the subbasin these data are overlaid on a hill shade DEM of the surrounding area. Each raster also shows the proportional difference in snow volume for the entire watershed on May 1<sup>st</sup> for each year. Calculations of proportional burn size and associated mean annual changes in SWE and total proportional losses are shown in the tables below the figure.

Table 5: Results of the model validation using field measurements of SWE collected from six of the burns between February and March of 2019. Percentage difference between the base/postfire albedo model were calculated against the field observations and the 95% confidence interval was included when  $n > 1$ . Instances where the postfire albedo model performed better than the base model are highlighted in green.

Fire	%Diff in SWED (Base)	%Diff in SWED (Postfire Albedo)	n
Horsethief Canyon	+61.06	+58.64	1
Bull	+24.67 ± 33.24%	+23.03 ± 33.79%	16
Boulder	+40.71 ± 22.03%	+41.22 ± 22.3%	9
Cliff Creek	+40.4 ± 26.93%	+41.17 ± 19.53%	13
Lava Mountain	+48.89 ± 24.08%	+46.18 ± 30.25%	8
Roosevelt	+59.79 ± 26.84%	+67.89 ± 23.91%	13
Overall	+40.22 ± 38.88%	+41.61 ± 46.29%	60

## REFERENCES

- Angers, V. A., Gauthier, S., Drapeau, P., Jayen, K., & Bergeron, Y. (2011). Tree mortality and snag dynamics in North American boreal tree species after a wildfire: A long-term study. *International Journal of Wildland Fire*, 20(6), 751. <https://doi.org/10.1071/wf10010>
- Armitage, R. P., Alberto Ramirez, F., Mark Danson, F., & Ogunbadewa, E. Y. (2013). Probability of cloud-free observation conditions across Great Britain estimated using Modis Cloud Mask. *Remote Sensing Letters*, 4(5), 427–435. <https://doi.org/10.1080/2150704x.2012.744486>
- Ashcroft, P. and F. J. Wentz. 2013. *AMSR-E/Aqua L2A Global Swath Spatially-Resampled Brightness Temperatures, Version 3*. Boulder, Colorado USA. NASA National Snow and Ice Data Center Distributed Active Archive Center. [http://dx.doi.org/10.5067/AMSR-E/AE\\_L2A.003](http://dx.doi.org/10.5067/AMSR-E/AE_L2A.003). Accessed July 18, 2015.
- Barnett, T., Malone, R., Pennell, W. et al. (2005). The Effects of Climate Change on Water Resources in the West: Introduction and Overview. *Climatic Change* 62, 1–11. doi:10.1023/B:CLIM.0000013695.21726.b8
- Barnett, T. P., Pierce, D. W., Hidalgo, H. G., Bonfils, C., Santer, B. D., Das, T., Bala, G., Wood, A. W., Nozawa, T., Mirin, A. A., Cayan, D. R., & Dettinger, M. D. (2008). Human-induced changes in the hydrology of the Western United States. *Science*, 319(5866), 1080–1083. <https://doi.org/10.1126/science.1152538>
- Brown, O. L. (1951). The Clausius-Clapeyron equation. *Journal of Chemical Education*, 28(8), 428. <https://doi.org/10.1021/ed028p428>
- Brown, J. K., & DeByle, N. V. (1987). Fire damage, mortality, and suckering in Aspen. *Canadian Journal of Forest Research*, 17(9), 1100–1109. <https://doi.org/10.1139/x87-168>
- Buchhorn, M., Smets, B., Bertels, L., De Roo, B., Lesiv, M., Tsendbazar, N.E., Linlin, L., Tarko, A. (2020): *Copernicus Global Land Service: Land Cover 100m: Version 3 Globe 2015-2019: Product User Manual*, Zenodo, Geneva, Switzerland, September 2020, doi:10.5281/zenodo.3938963
- Campagnolo, M. L., Sun, Q., Liu, Y., Schaaf, C., Wang, Z., & Román, M. O. (2016). Estimating the effective spatial resolution of the operational BRDF, albedo, and nadir reflectance products from Modis and VIIRS. *Remote Sensing of Environment*, 175, 52–64. <https://doi.org/10.1016/j.rse.2015.12.033>

- Cescatti, A., Marcolla, B., Santhana Vannan, S. K., Pan, J. Y., Román, M. O., Yang, X., Ciais, P., Cook, R. B., Law, B. E., Matteucci, G., Migliavacca, M., Moors, E., Richardson, A. D., Seufert, G., & Schaaf, C. B. (2012). Intercomparison of Modis albedo retrievals and in situ measurements across the Global Fluxnet Network. *Remote Sensing of Environment*, *121*, 323–334. <https://doi.org/10.1016/j.rse.2012.02.019>
- Colbeck, S. C. (1982). An overview of seasonal snow metamorphism. *Reviews of Geophysics*, *20*(1), 45. <https://doi.org/10.1029/rg020i001p00045>
- Danielson, J. J., & Gesch, D. B. (2011). *Global Multi-resolution Terrain Elevation Data 2010 (GMTED2010)* [Manual]. Reston, VI: USGS.
- Domine, F., Taillandier, A., Houdier, S., Parrenin, F., Simpson, W. R., & Douglas, T. A. (2006). Interactions between snow metamorphism and climate: Physical and chemical aspects. SPECIAL PUBLICATION-ROYAL SOCIETY OF CHEMISTRY, *311*, 27.
- Frankson, R., K. Kunkel, L. Stevens, D. Easterling, and B. Stewart. (2017). 2017: *Wyoming State Climate Summary. NOAA Technical Report. NESDIS 149-WY*, 4 pp.
- Hall, D. K., & Riggs, G. A. (2007). Accuracy assessment of the modis snow products. *Hydrological Processes*, *21*(12), 1534–1547. <https://doi.org/10.1002/hyp.6715>
- Hallema, D. W., Sun, G., Caldwell, P. V., Norman, S. P., Cohen, E. C., Liu, Y., Bladon, K. D., & McNulty, S. G. (2018). Burned forests impact water supplies. *Nature Communications*, *9*(1). <https://doi.org/10.1038/s41467-018-03735-6>
- Harpold, A. A. (2016). Diverging sensitivity of soil water stress to changing snowmelt timing in the western U.S. *Advances in Water Resources*, *92*, 116–129. <https://doi.org/10.1016/j.advwatres.2016.03.017>
- Hiemstra, C. A., Liston, G. E., & Reiners, W. A. (2006). Observing, modelling, and validating snow redistribution by wind in a wyoming upper treeline landscape. *Ecological Modelling*, *197*(1-2), 35–51. <https://doi.org/10.1016/j.ecolmodel.2006.03.005>
- Gersh, M., Gleason, K.E., Surunis, A. (2022). Forest fire effects on landscape snow albedo recovery and decay. *Remote Sensing*. Manuscript submitted for publication.
- Gleason, K. E., Nolin, A. W., & Roth, T. R. (2013). Charred forests increase snowmelt: Effects of burned woody debris and incoming solar radiation on snow ablation. *Geophysical Research Letters*, *40*(17), 4654-4661. doi:10.1002/grl.50896

- Gleason, K. E., & Nolin, A. W. (2016). Charred forests ACCELERATE snow Albedo Decay: Parameterizing the post-fire radiative forcing on snow for three years following fire. *Hydrological Processes*, 30(21), 3855-3870. doi:10.1002/hyp.10897
- Gleason, K. E., McConnell, J. R., Arienzo, M. M., Chellman, N., & Calvin, W. M. (2019). Four-fold increase in solar forcing on snow in western U.S. burned forests since 1999. *Nature Communications*, 10(1). doi:10.1038/s41467-019-09935-y
- Kulakowski, D., & Jarvis, D. (2011). The influence of mountain pine beetle outbreaks and drought on severe wildfires in northwestern Colorado and southern Wyoming: A look at the past century. *Forest Ecology and Management*, 262(9), 1686–1696. <https://doi.org/10.1016/j.foreco.2011.07.016>
- Liston, G. E., & Elder, K. (2006a). A distributed snow-evolution modeling system (SnowModel). *Journal of Hydrometeorology*, 7(6), 1259–1276. <https://doi.org/10.1175/jhm548.1>
- Liston, G. E., & Elder, K. (2006b). A meteorological distribution system for high-resolution terrestrial modeling (MicroMet). *Journal of Hydrometeorology*, 7(2), 217–234. <https://doi.org/10.1175/jhm486.1>
- Liston, G. E., Haehnel, R. B., Sturm, M., Hiemstra, C. A., Berezovskaya, S., & Tabler, R. D. (2007). Simulating complex snow distributions in windy environments using snowtran-3d. *Journal of Glaciology*, 53(181), 241–256. <https://doi.org/10.3189/172756507782202865>
- Liston, G. E., Hiemstra, C. A., Elder, K., & Cline, D. W. (2008). Mesocell study area snow distributions for the Cold Land Processes Experiment (CLPX). *Journal of Hydrometeorology*, 9(5), 957–976. <https://doi.org/10.1175/2008jhm869.1>
- Luce, C. H., & Holden, Z. A. (2009). Declining annual streamflow distributions in the Pacific Northwest United States, 1948–2006. *Geophysical Research Letters*, 36(16). <https://doi.org/10.1029/2009gl039407>
- Luce, C. H., Abatzoglou, J. T., & Holden, Z. A. (2013). The missing mountain water: Slower westerlies decrease orographic enhancement in the Pacific Northwest USA. *Science*, 342(6164), 1360–1364. <https://doi.org/10.1126/science.1242335>
- Luce, C. H., Lopez-Burgos, V., & Holden, Z. (2014). Sensitivity of snowpack storage to precipitation and temperature using spatial and temporal analog models. *Water Resources Research*, 50(12), 9447–9462. <https://doi.org/10.1002/2013wr014844>
- Lundquist, J. D., Dickerson-Lange, S. E., Lutz, J. A., & Cristea, N. C. (2013). Lower Forest density enhances snow retention in regions with warmer winters: A global

- framework developed from plot-scale observations and modeling. *Water Resources Research*, 49(10), 6356–6370. <https://doi.org/10.1002/wrcr.20504>
- Meromy, L., Molotch, N. P., Link, T. E., Fassnacht, S. R., & Rice, R. (2012). Subgrid variability of snow water equivalent at operational snow stations in the Western USA. *Hydrological Processes*, 27(17), 2383–2400. <https://doi.org/10.1002/hyp.9355>
- Mitchell, R. J., Freeman, K. M., & Yearsley, J. R. (2018). Modeling the effects of climate change on hydrology and stream temperature in the North Fork of the Stillaguamish River Basin. *Geological Society of America Abstracts with Programs*. <https://doi.org/10.1130/abs/2018am-323143>
- Molotch, N. P., & Bales, R. C. (2005). Scaling snow observations from the point to the grid element: Implications for observation network design. *Water Resources Research*, 41(11). <https://doi.org/10.1029/2005wr004229>
- Moriassi, D. N., Arnold, J. G., Van Liew M. W., Bingner, R. L., Harmel, R. D., & Veith, T. L. (2007). Model evaluation guidelines for systematic quantification of accuracy in watershed simulations. *Transactions of the ASABE*, 50(3), 885–900. <https://doi.org/10.13031/2013.23153>
- MTBS Data Access: Fire Level Geospatial Data. (2017, July - last revised). MTBS Project (USDA Forest Service/U.S. Geological Survey). Available online: <http://mtbs.gov/direct-download> [2017, July12].
- Musselman, K. N., Molotch, N. P., & Brooks, P. D. (2008). Effects of vegetation on snow accumulation and ablation in a mid-latitude sub-alpine forest. *Hydrological Processes*, 22(15), 2767–2776. <https://doi.org/10.1002/hyp.7050>
- National Centers for Environmental Information (NOAA-CDO). Climate Data Online. <https://www.ncdc.noaa.gov/cdo-web/> (Accessed on January 16, 2022)
- Nash, J. E., & Sutcliffe, J. V. (1970). River flow forecasting through conceptual models part I — a discussion of Principles. *Journal of Hydrology*, 10(3), 282–290. [https://doi.org/10.1016/0022-1694\(70\)90255-6](https://doi.org/10.1016/0022-1694(70)90255-6)
- Nolin, A. W., & Daly, C. (2006). Mapping “At Risk” snow in the Pacific Northwest. *Journal of Hydrometeorology*, 7(5), 1164–1171. doi:10.1175/jhm543.1
- Painter, T. H., Berisford, D. F., Boardman, J. W., Bormann, K. J., Deems, J. S., Gehrke, F., Hedrick, A., Joyce, M., Laidlaw, R., Marks, D., Mattmann, C., McGurk, B., Ramirez, P., Richardson, M., Skiles, S. M. K., Seidel, F. C., & Winstral, A. (2016). The airborne snow observatory: Fusion of scanning lidar, Imaging Spectrometer,

- and physically-based modeling for mapping snow water equivalent and Snow Albedo. *Remote Sensing of Environment*, 184, 139–152. <https://doi.org/10.1016/j.rse.2016.06.018>
- Riggs, G. A., Hall, D. K., & Román, M. O. (2017). Overview of NASA's Modis and viirs snow-cover Earth SystemData Records. <https://doi.org/10.5194/essd-2017-25>
- Roth, T. R., & Nolin, A. W. (2017). Forest impacts on snow accumulation and ablation across an elevation gradient in a temperate montane environment. *Hydrology and Earth System Sciences*, 21(11), 5427–5442. <https://doi.org/10.5194/hess-21-5427-2017>
- Ryan, S. E., Dwire, K. A., & Dixon, M. K. (2011). Impacts of wildfire on runoff and sediment loads at Little Granite Creek, western Wyoming. *Geomorphology*, 129(1-2), 113–130. <https://doi.org/10.1016/j.geomorph.2011.01.017>
- Saha, S., et al. (2011). *NCEP Climate Forecast System Version 2 (CFSv2) 6-hourly Products*. Research Data Archive at the National Center for Atmospheric Research, Computational and Information Systems Laboratory. <https://doi.org/10.5065/D61C1TXF>. Accessed 2021-05-13.
- Serreze, M. C., Clark, M. P., Armstrong, R. L., McGinnis, D. A., & Pulwarty, R. S. (1999). Characteristics of the Western United States snowpack from snowpack telemetry (SNOTEL) data. *Water Resources Research*, 35(7), 2145–2160. <https://doi.org/10.1029/1999wr900090>
- Sexstone, G. A., Clow, D. W., Fassnacht, S. R., Liston, G. E., Hiemstra, C. A., Knowles, J. F., & Penn, C. A. (2018). Snow sublimation in mountain environments and its sensitivity to forest disturbance and climate warming. *Water Resources Research*, 54(2), 1191–1211. <https://doi.org/10.1002/2017wr021172>
- Ueyama, M., Ichii, K., Iwata, H., Euskirchen, E. S., Zona, D., Rocha, A. V., Harazono, Y., Iwama, C., Nakai, T., & Oechel, W. C. (2014). Change in surface energy balance in Alaska due to fire and spring warming, based on upscaling eddy covariance measurements. *Journal of Geophysical Research: Biogeosciences*, 119(10), 1947–1969. <https://doi.org/10.1002/2014jg002717>
- U.S. Army Corps of Engineers, Hydrologic Engineering Center (USACE-HEC). 2012. *HEC-HMS Hydrologic Modeling System, User's Manual, Version 4.0, CPD-74A*. Hydrologic Engineering Center, Davis, CA.
- USDA Natural Resources Conservation Service. (USDA-NRCC) (2020). *SNOWpack TELEmetry Network (SNOTEL). Ag Data*

Commons. <https://data.nal.usda.gov/dataset/snowpack-telemetry-network-snotel>. Accessed 2021-03-11.

- U.S. Geological Survey, 2016, National Water Information System data available on the World Wide Web (USGS Water Data for the Nation), accessed [June 10th, 2022], at URL [<http://waterdata.usgs.gov/nwis/>]
- U.S. Geological Survey, 2019, National Hydrography Dataset (ver. USGS National Hydrography Dataset Best Resolution (NHD) for Hydrologic Unit (HU) 12 - 2001 (published 2019-10-02), accessed October 23, 2019 at URL <https://www.usgs.gov/national-hydrography/access-national-hydrography-products>
- Varhola, A., Coops, N. C., Weiler, M., & Moore, R. D. (2010). Forest canopy effects on snow accumulation and ablation: An integrative review of empirical results. *Journal of Hydrology*, 392(3-4), 219–233. <https://doi.org/10.1016/j.jhydrol.2010.08.009>
- West, A. M., Kumar, S., & Jarnevich, C. S. (2015). Regional modeling of large wildfires under current and potential future climates in Colorado and Wyoming, USA. *Climatic Change*, 134(4), 565–577. <https://doi.org/10.1007/s10584-015-1553-5>
- Westerling, A. L., Hidalgo, H. G., Cayan, D. R., & Swetnam, T. W. (2006). Warming and earlier spring increase western U.S. forest wildfire activity. *Science*, 313(5789), 940–943. <https://doi.org/10.1126/science.1128834>
- Westerling, A. L. R. (2016). Increasing western US forest wildfire activity: Sensitivity to changes in the timing of Spring. *Philosophical Transactions of the Royal Society B: Biological Sciences*, 371(1696), 20150178. <https://doi.org/10.1098/rstb.2015.0178>
- Western Regional Climate Center. (WRCC) (2021). *RAWS USA Climate Archive*. Retrieved from <https://raws.dri.edu>
- Wiscombe, W. J., & Warren, S. G. (1980). A model for the spectral albedo of snow. I: Pure snow. *Journal of the Atmospheric Sciences*, 37(12), 2712–2733. [https://doi.org/10.1175/1520-0469\(1980\)037<2712:amftsa>2.0.co;2](https://doi.org/10.1175/1520-0469(1980)037<2712:amftsa>2.0.co;2)
- Yuan, X., Wood, E. F., Luo, L., & Pan, M. (2011). A first look at Climate Forecast System version 2 (CFSV2) for hydrological seasonal prediction. *Geophysical Research Letters*, 38(13). <https://doi.org/10.1029/2011gl047792>

## **APPENDIX A: LONG-TERM POSTFIRE RECOVERY TREND METHODS**

Prior to running SnowModel and applying the postfire recovery parameterization, long-term recovery trends in albedo and landcover recovery were determined using remote sensing data from the study region. Albedo decay models were derived from MODIS MOD10A1 snow albedo data retrieved and pre-processed by Gersh and Gleason (Gersh & Gleason, 2022). MOD10A1 snow albedo is of 500m pixel resolution and is available on a daily basis. Pixel values within the burn regions were extracted for each day and cross-referenced with the MTBS burn severity data to determine the burn severity of each pixel. Due to the difference in image resolution between MTBS data and MODIS data (30m and 500m, respectively) the MTBS and MOD10A1 data were resampled to 250m and then burn severity values from MTBS were joined with the respective MOD10A1 snow albedo value for that pixel area.

To develop models of snow albedo decay as a function of days since snowfall, snow albedo data were classified according to their associated burn severity levels and years since fire. All pixels with negative years since fire values were classified as pre-fire. Snow depth data was retrieved from the nine SNOTEL stations contained within the study region via the National Weather and Climate Center (NWCC) data retrieval tool, averaged across all stations by date, and differenced using a lag time of 1 day to produce an average per day difference in snow depth for the entire study region. Snow days were classified as days where snow depth increased by 5cm or more since the previous day using base R. The “days since snowfall” data were then joined with the extracted snow albedo values in such a way that each snow albedo data point was associated with the number of days since snowfall.

A generalized linear model using a Gaussian distribution and a link log was then derived from these data using days since snowfall as the predictor variable and resulting snow albedo as the response. Several different factoring variables were used to identify key trends in the recovery of snow albedo decay over years since fire. Postfire data was split into three epochs (0-6 years postfire, 7-10 years postfire, and 11-15 years postfire) based on findings from Gersh and Kelly (2022). Albedo decay models were also computed as a function of burn severity. Finally, albedo decay models for buffer zones outside the burn regions were computed to determine significant differences in snow albedo between unburned and burned regions. Several Tukey plots were then produced using *ggplot2* to identify key factors in predicting snow albedo decay in burned regions.

Following Tukey plot analysis, it was found that pre-fire and postfire explained the most variance in snow albedo decay and thus factors of landcover and years since fire were excluded. Two final models were produced using the generalized linear log model: one for the pre-fire snow albedo values and one for the postfire snow albedo values. Each of the individual models was tested for significance using a t-test and then analysis of variance was computed between the two models using a Wald test. Stepwise functions based on years since fire were then computed such that snow albedo decay would recover to pre-burn levels over 15 years. This was done by creating 13 equally-sized steps between the parameters of the post-burn snow albedo decay function and the pre-burn snow albedo decay function. These models would then be used later in SnowModel to simulate the recovery of snow albedo decay over the course of 15 years following burn.

## **APPENDIX B: TUKEY ANALYSIS OF LONG TERM POSTFIRE RECOVERY**

### **TRENDS**

Prior to modeling burned albedo decay, I set out to identify key differentiating trends in snow albedo within and without the burn region. MOD10A1 surface snow albedo data was grouped by landcover and years since burn and analyzed using two Tukey plots (Figure A1 and Figure A2). Tukey plot comparison within the burn regions showed similar long term albedo values regardless of burn severity (Figure A1). Pixels classified as high and medium burns showed no significant difference from one another for up to 15 years following fire. Low severity burned pixels only showed a significant difference from high burn pixels in the first 6 years following fire and showed no significant difference from moderate burn pixels for the entire period. These findings provided the rationale that burned pixels, regardless of MTBS burn severity classifications, can be grouped into a single classification. Comparison of open pixels with low, medium and high severity burned pixels showed significant differences over the entire time period. Further, burned pixels seemed to trend towards albedo values similar to open regions over the course of the time range. These two findings led to two important conclusions: 1) burned areas have similar surface snow albedo values to one another in the long term, regardless of burn severity, and thus can be grouped and classified as one and 2) burned pixels trend towards open area surface snow albedo values in the long term, thus providing the rationale for incorporating a recovery mechanic in the SnowModel parameterizations to come.

To justify using a modified snow albedo decay function for burned pixels, it was necessary to identify significant differences between snow surface albedo values within

the burn and outside the burn regions. Tukey plots comparing snow surface albedos in the burn regions to snow surface albedos outside the burn regions were constructed (Figure A2). For this figure, burned pixels were grouped into a single “Burn” group based on the reasoning above and these pixels showed significant differences from snow surface albedo values outside in the buffer regions outside the burns. Tukey analysis showed all groups (buffer forest, buffer open, burned, and open within burn) were significantly different from one another across all time periods. Burned pixels exhibited significantly lower SSA than buffer open pixels 0-6 years PF, no significant difference between 6-10 years PF, and significantly higher SSA 10+ PF. This indicated that although burned forests have lower SSA immediately following fire, they eventually recover to a state similar to that of an unburned open region in the long term. This observation is further supported by comparison to burned forests with unburned forests. Burned forests exhibited significantly higher SSA values than unburned forests at all time periods and the gap between these two landscape types widened in the longer term. Together these observations show that SSA in burned forests increasingly deviate from forest SSA values and approach and overtake SSA values in open regions. Following a burn, forest canopy is removed and burned forests become more like open regions in the decades following fire. Analysis of the Tukey plots provided the rationale for creating differing albedo decay models for pre-burn and post-burn pixels. Further, SSA trends approach levels similar to open regions in the long term, thus snow albedo decay should recover to pre-burn albedo decay levels of open regions in the long term.

Following Tukey plot analysis of the MOD10A1 data, albedo decay models were computed for both pre-fire and postfire pixels and divided into accumulation and ablation

periods (Figure A3). Exponential decay models were computed using a generalized linear model with a Gaussian log-link (Table 6). Both the pre-fire and postfire models were found to be significant using a t-test. When separated into accumulation and ablation submodels, pre- and postfire accumulation albedo decay were found to be significantly different using a Wald test. Likewise, pre- and postfire ablation albedo decay models were found to be significantly different to high degree using a Wald test. Snow albedo was plotted as a function of days since snowfall measured using SNOTEL snow depths. Separate albedo decay models were computed for accumulation and ablation periods as snow metamorphism has been shown to accelerate much more rapidly during the ablation period than during accumulation. During accumulation, pre- and postfire albedo decay showed similar decay rates, but postfire albedo was higher at all days following fresh snowfall. This is likely due to the fact that the solar incidence angle during early winter is lower, thus temperature gradients within the snowpack are substantially lower during the accumulation period and the postfire effects on snow albedo are not significant in comparison to the postfire removal of canopy cover. During ablation, the initial albedo following snowfall is higher than pre-fire SSA, but decays at a much faster rate. This aligns well with findings in the literature as, during ablation (April 1<sup>st</sup> till snow disappearance), the solar incidence angle is much higher and additional absorption of shortwave radiation caused by postfire introductions of black carbon into the snowpack are more significant than in the accumulation period. This creates greater temperature gradients that accelerate snow metamorphism and result in faster decay of snow albedo in the days following fresh snowfall.

## APPENDIX C: FIGURES AND TABLES

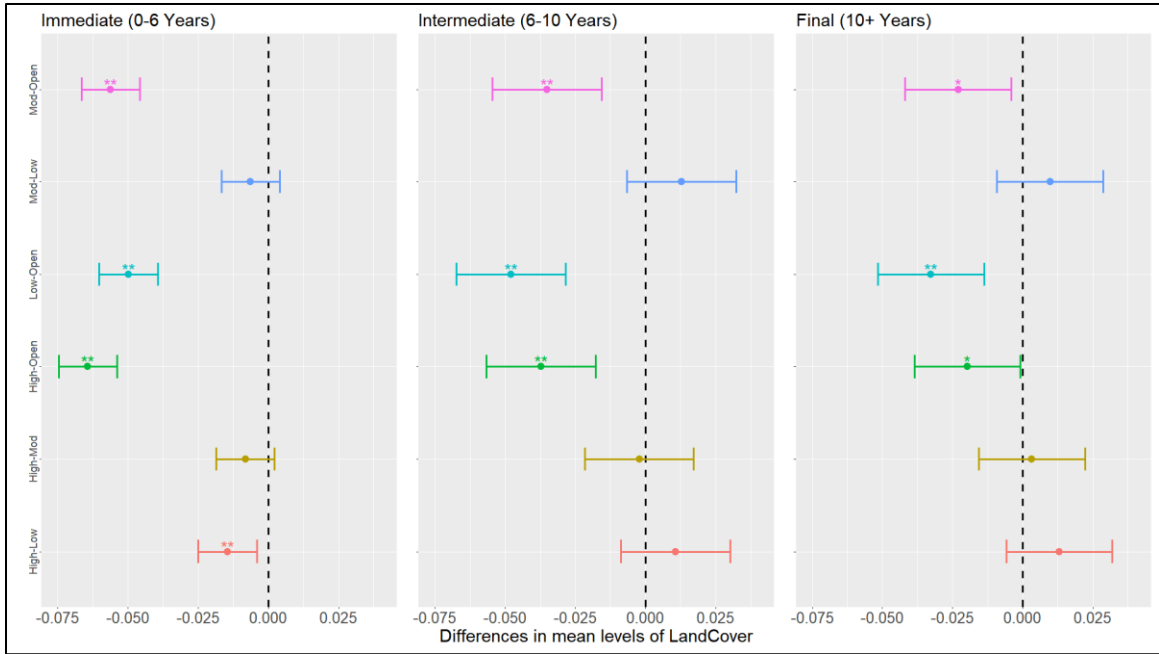


Figure A1: A Tukey plot of differences in mean MOD10A1-measured snow albedo data in comparison to burn severity within the burn regions. The plots are split into different periods following the burn based on significant snow albedo recovery partitions from Gersh and Gleason, 2021. The y-axis shows which landcover types are being compared and the plot shows the relative difference mean albedo between the first landcover type and the second landcover type.

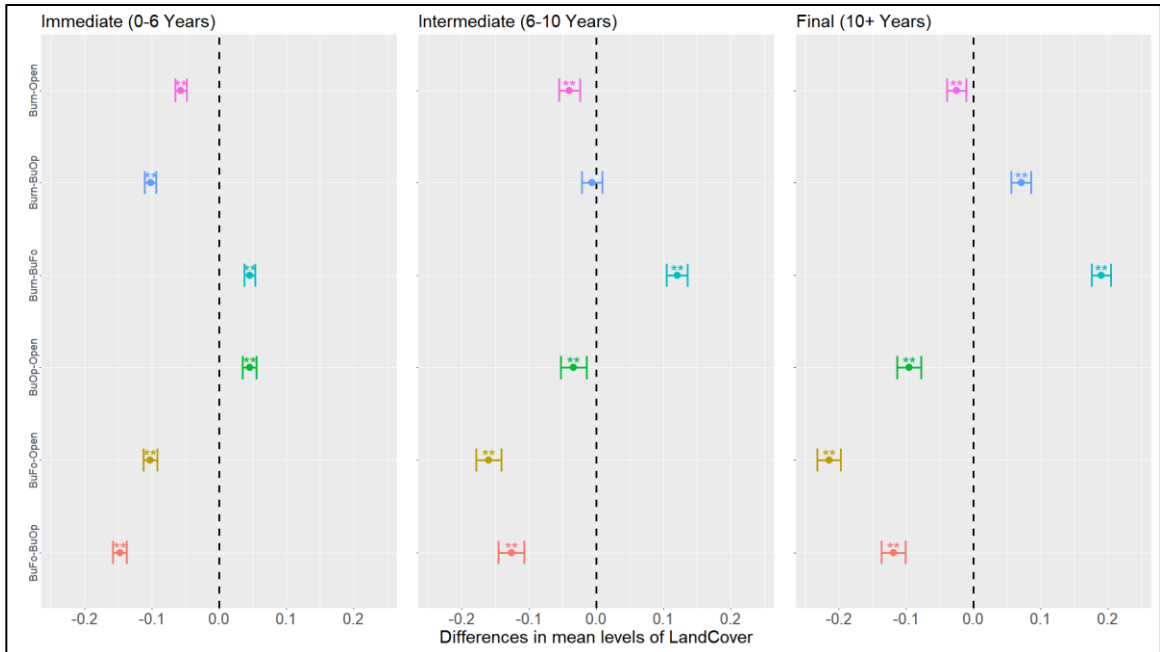


Figure A2: A Tukey plot of differences in mean MOD10A1-measured snow albedo data in comparison to burn severity between regions outside the burn areas and regions inside the burn areas. All burn types were combined into a single “Burn” group. Open areas within the burn are titled “Open”. Buffer forest and buffer open areas outside the burn are titled “BuFo” and BuOp”, respectively.

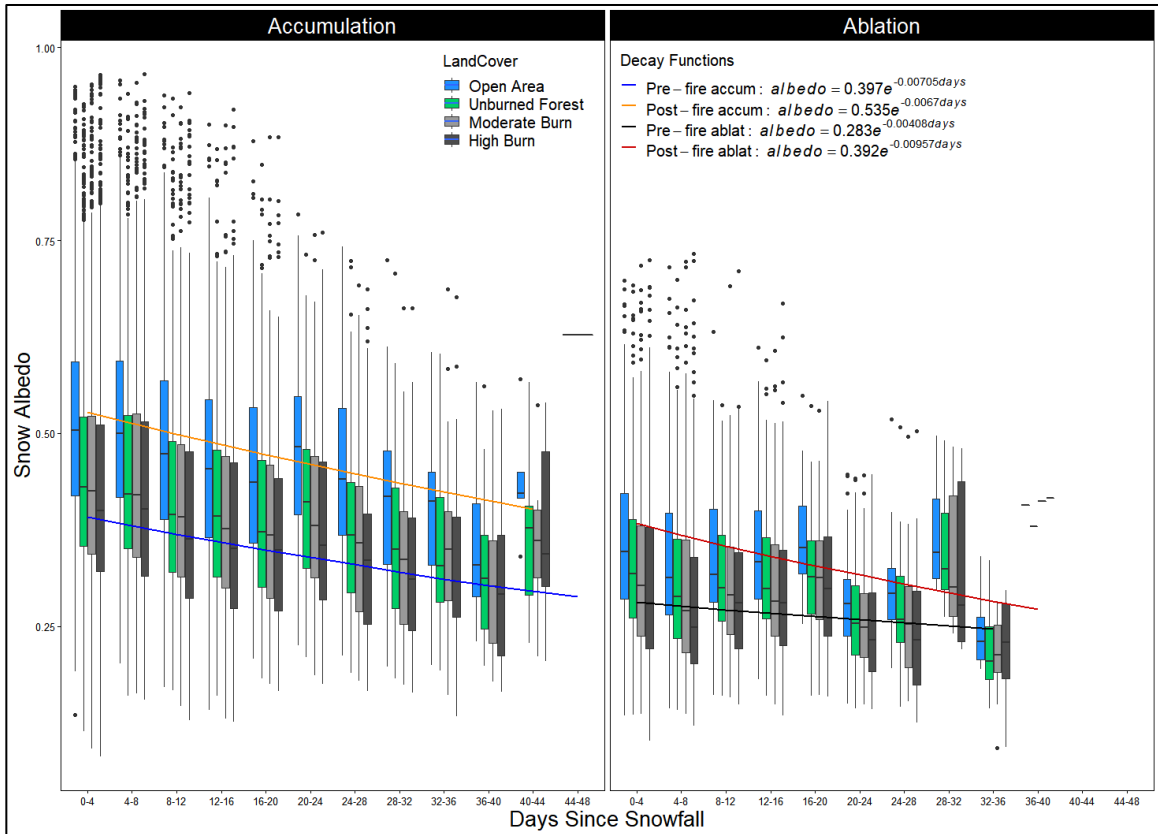


Figure A3: The results of the snow albedo decay generalized linear model with snow albedo as a function of days since last snowfall. Box plots showing the distribution of the snow albedo of pixels within the burn region separated by landcover type are underlaid behind the decay functions. Four decay functions were computed (pre-fire accumulation, pre-fire ablation, postfire accumulation, and postfire ablation) and the coefficients of these functions are included within the plot.

Table A1: Numerical results of significance testing performed on all modeled SWE results. For each result, 100 random pixels between the base model and postfire albedo model were selected and a two-sided Welch Two-Sample t-test was performed with an alpha value of 0.05.

Immediate Losses p-values Welch Two-Sample t-test; two-sided; $\alpha = 0.05$ ; $n = 100$								
	Boulder	Green Knoll	Purdy	Bull	Horsethief Canyon	Lava Mountain	Cliff Creek	Roosevelt
p-value	1.58E-04	0.0479	0.0016	0.438	1.12E-05	3.21E-18	1.99E-06	0.00261
Total Losses p-values Welch Two-Sample t-test; two-sided; $\alpha = 0.05$ ; $n = 100$								
	Boulder	Green Knoll	Purdy	Bull	Horsethief Canyon	Lava Mountain	Cliff Creek	Roosevelt
p-value	0.086	4.42E-04	0.420	0.0134	0.0045	1.71E-03	0.0041	0.0062
Period Averaged Peak SWE p-values Welch Two-Sample t-test; two-sided; $\alpha = 0.05$ ; $n = 100$								
	Boulder	Green Knoll	Purdy	Bull	Horsethief Canyon	Lava Mountain	Cliff Creek	Roosevelt
Period 1	1.35E-33	1.39E-33	0.00270	3.71E-04	6.22E-15	0.450	0.811	0.00559
Period 2	3.59E-07	8.04E-17	0.00436	5.23E-18	0.00367	0.00498	4.30E-05	
Period 3	0.00960	0.0023	3.22E-06	0.207	0.245			
Period 4	1.58E-22	0.0744	1.26E-14	0.834				
Period 5	0.414	0.00408	2.17E-08					
Post-Rec.	1.35E-08	4.74E-27						
March 1st SWE p-values Welch Two-Sample t-test; two-sided; $\alpha = 0.05$ ; $n = 100$								
	Boulder	Green Knoll	Purdy	Bull	Horsethief Canyon	Lava Mountain	Cliff Creek	Roosevelt
Period 1	4.84E-59	2.45E-34	2.82E-21	1.08E-25	1.23E-31	0.156	0.247	0.0176
Period 2	0.501	2.69E-24	1.29E-44	1.77E-18	1.66E-13	7.21E-47	1.61E-24	
Period 3	0.0406	4.80E-06	2.23E-27	0.213	9.84E-07			
Period 4	0.381	2.86E-13	0.0494	2.96E-25				
Period 5	0.00444	1.19E-05	6.21E-61					
Post-Rec.	4.94E-52	9.17E-44						
April 1st SWE p-values Welch Two-Sample t-test; two-sided; $\alpha = 0.05$ ; $n = 100$								
	Boulder	Green Knoll	Purdy	Bull	Horsethief Canyon	Lava Mountain	Cliff Creek	Roosevelt
Period 1	0.00152	2.77E-29	7.66E-09	2.90E-06	2.34E-17	3.20E-07	0.00245	0.144
Period 2	0.813	1.64E-20	0.00812	0.0328	0.0600	0.0159	0.0224	
Period 3	0.00679	0.574	0.101	2.36E-05	0.290			
Period 4	7.48E-19	9.67E-11	3.39E-23	0.0336				
Period 5	1.26E-05	0.109	3.01E-12					
Post-Rec.	1.13E-16	2.72E-08						
May 1st SWE p-values Welch Two-Sample t-test; two-sided; $\alpha = 0.05$ ; $n = 100$								
	Boulder	Green Knoll	Purdy	Bull	Horsethief Canyon	Lava Mountain	Cliff Creek	Roosevelt
Period 1	4.52E-101	4.07E-61	0.546	3.80E-05	5.39E-22	0.383	1.17E-07	4.27E-11
Period 2	1.63E-56	3.11E-30	0.0279	3.32E-27	2.42E-06	2.35E-12	3.01E-14	
Period 3	1.20E-19	0.232	0.199	0.0157	6.48E-08			
Period 4	1.09E-08	2.22E-04	5.82E-23	0.846				
Period 5	0.204	9.76E-18	0.00342					
Post-Rec.	1.58E-26	2.93E-06						

Table A2: Table showing the results of the generalized linear log-link model performed to calculate albedo decay models for burned and unburned regions using MODIS-MOD10A1 surface snow albedo data collected by Gersh et al. (2022). A Wald test was carried out to determine significant differences between the accumulation and ablation models for pre- and postfire periods. The results of the Wald test (standard error, Wald Z score, and p-value) are shown on the second table.

<b>Generalized Linear Model</b>			
<b>Period</b>	<b>n</b>	<b>t</b>	<b>p</b>
Pre-fire	12537	-16.94	2E-16
Post-fire	12066	-20.81	2E-16
<b>Wald test</b>			
<b>Model</b>	<b>SE</b>	<b>Wald Z</b>	<b>P</b>
Accumulation (pre-fire vs. post-fire)	0.006	49.82	<0.0001
Ablation (pre-fire vs. post-fire)	0.013	24.92	<0.0001